Eur. Phys. J. C (2025) 85:782
https://doi.org/10.1140/epjc/s10052-025-14500-7

THE EUROPEAN PHYSICAL JOURNAL C

Regular Article - Theoretical Physics

Bulk viscous matter interacting with decaying vacuum energy density: a model for late-time evolution of the Universe

Tanmay Nandi[a], **Amitava Choudhuri**[b]

Department of Physics, The University of Burdwan, Golapbag, Purba Bardhaman, West Bengal 713104, India

Received: 9 April 2025 / Accepted: 5 July 2025

Abstract The late-time cosmological expansion within a flat Friedmann–Lemaître–Robertson–Walker (FLRW) spacetime is studied using a model characterized by bulk viscous dark matter (bulk viscosity $\zeta = \zeta_0\rho_m H^{-1} + \zeta_1 H$, ζ_0 & ζ_1 are constants, and H, the Hubble parameter) interacting with a decaying vacuum density $\rho_\Lambda = \mathcal{C}_0 + 3\nu H^2$, where $\mathcal{C}_0$ and ν are constants. The bulk viscous pressure is described by Eckart's theory. The interaction term is defined as $Q = 3H\alpha(\rho_m + \rho_\Lambda)$, where α, the interaction parameter. Analytical solutions for the Hubble parameter and the scale factor have been derived. The validity of the models is evaluated by constraining their free parameters using observational data from *Cosmic Chronometer*, the *Pantheon*, and a combination of both datasets. The goodness of fit is assessed by minimizing the χ^2 function utilizing the Markov Chain Monte Carlo (MCMC) method. Selection information criteria, namely AIC and BIC, have been obtained to analyze the models' stability. Additionally, several essential cosmological parameters characterizing the evolution dynamics are estimated and discussed analytically, and compared with the ΛCDM model. The proposed model suggests a transition from the deceleration to the acceleration phase, indicating thermodynamic equilibrium in the distant future, aligning with the ΛCDM model. The model shows a slight deviation from ΛCDM model and effectively reduces the H_0 tension between local measurements by $R21$ and global measurements by Planck 2018. The model is consistent with thermodynamic laws and upholds the second law of thermodynamics. Finally, Phase-space analysis supports the same evolutionary transitional phases.

1 Introduction

The discovery of late-time cosmic acceleration has initiated a new research trajectory in contemporary cosmology [1,2]. A range of observational studies, including those examining type Ia supernovae [3–5], the large-scale structure (LSS) of the universe [6,7], the cosmic microwave background (CMB) [8], and baryon acoustic oscillations (BAO) [9], corroborate this phenomenon. This acceleration is not adequately accounted for by the matter and radiation currently present in the universe. Broadly, two primary categories of models have been proposed: one that modifies the geometric components of Einstein's field equations (EFE) and another that alters the right-hand side of Einstein's equation through a specific formulation of the energy-momentum tensor $T_{\mu\nu}$, which introduces a significant degree of negative pressure [10]. With respect to the aforementioned modification, scientists have recognized a specific form of energy that generates a repulsive gravitational influence, thus promoting the acceleration of the universe. Data from the Wilkinson Microwave Anisotropy Probe (WMAP) [11,12] and large-scale structure observations from the Sloan Digital Sky Survey (SDSS) [13,14] provide evidence for the existence of dark energy (DE). Cosmological assessments of these findings suggest that the universe is composed of approximately 70% DE, 30% dust matter (including cold dark matter and baryons), and minimal radiation [15]. Notable candidates for dark energy include the cosmological constant, phantom energy, quintessence, and Chaplygin gas. The cosmological constant, frequently denoted as Lambda-cold-dark matter (ΛCDM), is considered the most compelling candidate for explaining cosmological observations, characterized by an equation of state (EoS) of $\omega = -1$ [16]. Nonetheless, it faces challenges such as the cosmological constant problem (the fine-tuning issue) [17,18] and the cosmic coincidence problem [19,20]. In order to address the challenges associated with the ΛCDM

[a] e-mail: tanmaynandi7@gmail.com
[b] e-mail: amitava_ch26@yahoo.com (corresponding author)

Published online: 19 July 2025

model and to investigate the accelerating universe, two primary subjects have surfaced in the literature: one pertains to bulk viscous cosmology, while the other concerns the varying cosmological constant.

Viscous fluid cosmology constitutes a pivotal research domain focused on elucidating the Universe's accelerated expansion [21]. It has long been recognized that a dissipative fluid can induce acceleration during the Universe's expansion phase. In an isotropic and homogeneous universe, dissipative processes are predominantly characterized by bulk viscosity, while heat dissipation and shear viscosity are typically neglected due to their incompatibility with the cosmological principle [22–24]. Viscosity in a cosmological fluid emerges when the fluid expands at a rate that precludes sufficient time for the system to reestablish local equilibrium, resulting in an effective pressure that aids in restoring the system to its local thermodynamic equilibrium. Once thermal equilibrium is reestablished, the bulk viscosity pressure dissipates [25,26]. In the realm of dissipative fluid dynamics, the connection between macroscopic and microscopic theories is facilitated by the transport coefficients of the matter. Bulk viscosity can be qualitatively interpreted as a macroscopic manifestation of frictional effects within the fluid, originating from molecular-like interactions at the microphysical level [27,28].

Research into isotropic, spatially flat, homogeneous viscous cosmological models has been conducted through both causal and non-causal theories. Within the framework of non-causal theory, Eckart [29] proposed that bulk viscous pressure perturbations can propagate at infinite speeds. This first-order non-causal viscous theory was subsequently revised by Landau and Lifshitz [30]. In contrast, the Full Israel-Stewart theory, a second-order model addressing the causality issue, was developed by Israel and Stewart [31]. Despite the challenges of causality, Eckart's theory is frequently employed due to its simplicity.

According to Eckart's theory [29], the bulk viscous pressure of the cosmic fluid is defined by the equation: $\Pi = -3\zeta H$, where ζ is the bulk viscous coefficient and H is the Hubble parameter. Bulk viscosity is a fundamental property of a system, influenced by its overall density and constituent components. Variations in temperature further impact these properties, leading to a general formulation of viscosity in relation to density and temperature [32]. It is commonly expressed as $\zeta = \zeta_0 \rho^s$, where ζ_0 is a positive constant [33,34]. This parameterization is particularly pertinent in cosmological models involving interacting dark energy and dissipative dark matter. Research indicates that a causal model with a dissipative dark matter component can exhibit an accelerated expansion phase for $s = 1/2$. However, scenarios with s values less than or greater than 1/2 do not support accelerated expansions [35–37]. Non-causal frameworks have permitted more generalized expressions of bulk viscosity, including dependencies on the Hubble parameter. Nonetheless, these approaches have not successfully demonstrated the conventional radiation-dominated or matter-dominated phases. A novel parameterization of bulk viscosity, expressed as $\zeta \sim H^{1-2s}\rho_m^s$, incorporates the dependence on both dark matter density and the Hubble parameter [38]. This new Ansatz suggests that the effects of bulk viscosity become significant primarily during cosmological stages dominated by dark matter, where its energy density is proportional to the bulk viscosity coefficient [39,40]. The specific case where $s = 0$ corresponds to a bulk viscosity coefficient of the form $\zeta \propto H$, which is typically associated with unified viscous models and dissipative dark matter. Conversely, when $s = 1$, the bulk viscosity coefficient takes the form $\zeta \propto H^{-1}\rho_m$, which may facilitate accelerated expansion. In this paper, we will adopt the following expression for the bulk viscosity coefficient in our analysis [41,42]

$$\zeta = \zeta_0 \rho_m H^{-1} + \zeta_1 H. \tag{1}$$

It is important to note that ζ_0 is a dimensionless quantity, while ζ_1 possesses the unit ML^{-1}.

On the other hand, numerous alternative theories have been proposed alongside the ΛCDM framework to address its limitations. Certain studies within the literature suggest that specific dynamical dark energy models may effectively mitigate the deficiencies of ΛCDM. Bertolami [43] and Ozer and Taha [44] introduced a cosmological model featuring a time-varying cosmological constant, positing it as a potential candidate for dark energy. In this context, models incorporating time-varying vacuum energy density (VED), often referred to as 'decaying vacuum cosmology,' are considered promising solutions to these challenges. Although a fundamental theory explaining time-varying vacuum energy remains unattained, a phenomenological approach has been developed to parameterize the cosmological constant. In a recent study by Rezaei et al. [45], the authors employed phenomenological reasoning to describe the time-dependent behavior of $\Lambda(t)$, representing it as a power series expansion of the Hubble rate and its time derivatives: $\Lambda(t) \propto H$, $\Lambda(t) \propto \dot{H}$, $\Lambda(t) \propto H^2$. Additionally, Singh and Solà [46] investigated Friedmann cosmology through the lens of the Brans-Dicke theory, focusing on a scenario where the vacuum density decreases over time. The authors specifically analyzed the function $\Lambda(t)$, which is expressed by the phenomenological equation $\Lambda(t) = \lambda + \sigma H$, where λ and σ are constants, and H represents the Hubble parameter. Khatri and Singh [47], also operating within the Brans-Dicke framework, aimed to impose constraints on models of time-varying vacuum energy. Numerous researchers have explored the concept of decaying vacuum energy, wherein the time-varying vacuum has been modeled phenomenologically [48–52]. The precise formulation of VED remains to be deter-

mined; however, quantum field theory (QFT) within a curved spacetime framework delineates the general evolution of vacuum energy density, ρ_Λ, as a function of the Hubble rate. In this context, Shapiro and Solà [53], and Solà [54], proposed a potential connection between cosmology and quantum field theory through the renormalization group (RG), leading to the concept of running vacuum models (RVM) characterized by VED. The RG method is formulated through the effective average action Γ_k, which is dependent on a momentum scale k [55,56]. This framework treats gravity as a quantum field theory, where the effective dynamics vary with scale, progressively incorporating quantum fluctuations. The RG flow equations illustrate how the dimensionless couplings-specifically, the Newton constant $G(k)$ and the cosmological constant $\Lambda(k)$-evolve as functions of k, converging towards fixed points that determine their behavior across different scales. A prevalent choice, supported by the homogeneity and isotropy of the universe, is to establish k as proportional to $1/t$, with t representing cosmological time. This relationship indicates that as t approaches 0 (near the big bang), k tends towards infinity, entering the fixed point regime where gravity becomes asymptotically free. Utilizing this identification, the running couplings are expressed as functions of time: $G(t) = G(k(t))$, $\Lambda(t) = \Lambda(k(t))$ [55]. As we have considered $c = 1, 8\pi G = 1$, thus we focus solely on $\Lambda(t)$. This approach specifically highlights an RG equation in which the change in ρ_Λ with respect to $H(t)$ involves only even powers of H, expressed as follows [57,58]:

$$\frac{d\rho_\Lambda}{d\ln H^2} = \frac{1}{(4\pi)^2}\sum_i \left(a_i M_i^2 H^2 + b_i H^4 + c_i \frac{H^6}{M_i^2} + \cdots\right), \tag{2}$$

where the coefficients $a_i, b_i, c_i...$ are dimensionless, and the M_i represent the masses of the particles in the loops. The dimensionless coefficients receive loop contributions from bosonic and fermionic matter fields with varying masses M_i. It is evident that the expansion (2) converges rapidly at low energy levels, where H remains relatively small-certainly much less than any particle mass. No additional term beyond H^2 (not even H^4) can make a substantial contribution on the right-hand side of Eq. (2) at any point in cosmological history prior to the Grand Unified Theory (GUT) scale $M_{\rm GUT}$, which is typically several orders of magnitude lower than the Planck scale $M_P \sim 10^{19}$ GeV. Nevertheless, during the very early universe, the effects of H^4 can also be considerable, along with the terms H^6/M_i^2 and those of higher order. The (dimensionless) coefficients receive loop contributions from boson and fermion matter fields of different masses M_i. Clearly, the expansion (2) converges very quickly at low energies, where H is rather small-certainly much smaller than any particle mass. Integrating the Eq. (2), we anticipate the following general type of (appropriately normalized) RVM density:

$$\rho_\Lambda(H) = c_0 + 3\nu H^2 + 3\gamma\frac{H^{n+2}}{H_I^n}, \tag{3}$$

where H_I is the Hubble parameter at inflation. The coefficients $\nu = \frac{1}{6\pi}\sum_{i=f,b} c_i \frac{M_i^2}{M_P^2}$, and $\gamma = \frac{1}{12\pi}\frac{H_I^2}{M_P^2}\sum_{i=f,b} b_i$ receive contributions from all the matter particles and function as one-loop β-functions for the RG running. The expanding universe at times after recombination, therefore, consists of dust ($\omega = 0$) plus the running vacuum fluid described by Eq. (3) with $H \ll H_I$. In this case, the H^{n+2} term ($n > 1$) is completely negligible compared to H^2. Thus (3) can be written as [59–61]:

$$\rho_\Lambda = \mathcal{C}_0 + 3\nu H^2, \tag{4}$$

where $\mathcal{C}_0 = 3H_0^2(\Omega_\Lambda - \nu)$ acts as the additive constant, defined by the boundary condition $\rho_\Lambda(H_0) = \rho_{\Lambda 0}$. The rationale for adopting a variable of this nature (4) is rooted in QFT [62]. This specific functional form of $\Lambda(t)$ has been employed to investigate the progression of the cosmic star formation rate and to impose constraints on the model parameters. Within this context, ν denotes the dimensionless vacuum parameter, which is anticipated to be exceedingly small, specifically $|\nu| \ll 1$. Consequently, a positive value of ν promotes the cosmic evolution of the vacuum [62,63].

The aforesaid analysis reveals that in a homogeneous and isotropic universe, neither a dynamical cosmological constant nor bulk viscosity can independently explain the current cosmological parameters. Numerous researchers have delved into viscous cosmological models, examining both constant and time-dependent cosmological constants [47,64–68]. For instance, Hu and Hu [67] investigated a model where bulk viscosity is proportional to the Hubble parameter, while Herrera-Zamorano et al. [68] focused on a dual-fluid cosmological model based on the Eckart formalism. In their findings, among the two fluids, one fluid functions as dark energy, replicating the dynamics of the cosmological constant, while the other fluid symbolizes dark matter, including a viscosity term. They also included a nuanced interaction between bulk viscous matter and cosmological constants in elucidating the universe's dynamics.

In the present study, we posit that the Universe consists of two principal components: a non-ideal, viscous dark matter and a decaying vacuum energy that interacts with the viscous dark matter. Most cosmological models posit that matter and DE interact solely through gravity [69], but the microphysics of the dark sector is still predominantly uncharted; various properties can be assessed or constrained by aligning theoretical predictions with CMB and LSS observations [70]. Dark matter's interactions with electrons or protons during the early Universe leave distinct marks on the CMB and

the matter power spectrum, which can be examined through cosmological and astrophysical observations [71]. Observa tions suggest that DE exerts a negative pressure on the energy budget, while DM's pressure is minimal, potentially nearing zero. The interaction between DE and baryons is insignificant [72], and the relationship between DE and radiation is complex, as photons do not follow geodesic trajectories. In contrast, an interaction between dark matter and dark energy is generally introduced through a phenomenological modification of the matter conservation equations, while the Einstein equations are preserved without change [73–75]. The interaction between DE and DM is likely minimal, as the concordance model fits the data exceptionally well. On the other hand, DM-DE interactions can address issues like the cosmic coincidence problem, cosmic doomsday scenarios from phantom energy [76], and the cosmic age problem linked to old quasars [77]. This non-gravitational interaction could have significant implications at both fundamental and cosmological levels. The true nature of these interactions may influence cosmological observables, particularly concerning the interaction between DM and DE [78–81]. Concurrently, cosmological and astrophysical observations can be effectively utilized to constrain any potential coupling between these two dark sectors. The thermodynamic properties of interaction models, as examined in [82,83], indicate that a non-zero chemical potential for at least one of the fluids enables the decay of the DM fluid into DE without contravening the second law of thermodynamics, and in certain instances, this is supported by cosmological data. Thus, studying interactions between these dark sectors is crucial, though it requires proposing and testing a phenomenological DE model due to a limited understanding of the micro-origin [84]. There is as yet no basis in fundamental theory for a specific coupling in the dark sector, and therefore any coupling model will necessarily be phenomenological, although some models will have a more physical justification than others [85]. Various models of energy exchange (interaction term Q) have been considered. Some of these are simple functional ansatzes, such as $Q \propto a^n$. However these models are incomplete: they cannot be thoroughly tested against observations, since one has no idea what the perturbation of Q should be [86]. In the literature, three primary categories are recognized for selecting the phenomenological energy exchange term Q. (i) Q is considered to be proportional to the Hubble rate, H, multiplied by either the energy densities, their total, or some alternative combination of the energy densities [80,87–90], such as $Q \propto H\rho_m$ [91,92] or $Q \propto H\rho_\Lambda$ [93] or $Q \propto 3H(\rho_m + \rho_\Lambda)$ [73,94–98] i.e,

$$Q = 3H\alpha(\rho_m + \rho_\Lambda), \tag{5}$$

where α represents the interaction parameter, the coupling constant. This assumption is supported by a quintessence model that results in a time-varying mass for dark matter particles [91]. (ii) Another common option for a phenomenological interaction is a constant multiplied by either of the energy densities or a combination thereof (excluding the Hubble parameter, thereby lacking an implicit time dependence) [85,99–101]. In different contexts, this form of interaction has been utilized to explain the decay of curvaton [102–104] or the generation of quintessence field condensation through a gradual decay of superheavy dark matter. (iii) A fascinating possibility also includes elastic scattering among the dark-sector 'particles', which does not result in energy exchange in the background. These models produce significantly milder observational signatures [105] .

In Ref. [106], the authors examine a model of interacting bulk viscosity defined by a diminishing vacuum density, where bulk viscosity is represented as $\zeta = \zeta_0$ and $\zeta = \zeta_0 + \zeta_1 H$. They investigated an interaction function that is proportional to the matter density, represented as $Q \propto \rho_m H$. In our analysis, we study a late-time expanding universe depicted by an interacting bulk viscous model featuring a decaying vacuum energy density. In this study, we consider bulk viscosity as given in (1) and VED as given in (4), while the interaction between DE and DM is provided in (5).

Significant research efforts have been devoted to examining empirical evidence from type Ia supernovae, CMB, BAO, and Hubble measurements, all of which are essential for the refinement of cosmological models. A Bayesian Markov Chain Monte Carlo (MCMC) [107] analysis is conducted to explore the parameter spaces of the model by employing three distinct combinations of observational data, particularly from type Ia supernovae (*Pantheon*) [108] and observational Hubble data (also referred to as *Cosmic Chronometer*). Furthermore, selection information criteria such as AIC and BIC are examined to evaluate the model's robustness.

A phase space encompasses all potential states concerning a system's position and momentum [109]. By analyzing this phase space, a deeper understanding of the dynamic properties of cosmological models can be achieved, thereby simplifying complex equations. This approach facilitates the investigation of various evolutionary trends by transforming equations into an autonomous format [110–112]. This analysis is pivotal as it focuses on critical points, which are crucial for evaluating the behavior of field equations. Critical points offer valuable insights into a model's temporal behavior and its association with the universe's evolutionary epochs. The stability of these phases is assessed through eigenvalue calculations at critical points, underscoring the significance of dynamical systems analysis in the context of dark energy [88,109,113].

The organization of this paper is as follows: In Sect. 2, we outline the core equations that describe the expansion dynamics within the FLRW universe, influenced by a barotropic bulk viscous fluid and a decaying VED. This section details

the derivation of the model equation and its analytical solution. Section 3 focuses on the analysis of *Pantheon* and observational Hubble data to derive constraints on the model's free parameters through MCMC analysis. The implications of these findings are discussed in Sect. 4, where we calculate important cosmological parameters, including the deceleration parameter, equation of state parameters, the statefinder pair, and the Om Diagnostic, along with their evolutionary behavior. Entropy evolution and the second law of thermodynamics are presented in Sect. 5. The phase space analysis are carried out in Sect. 6. Section 7 concludes with final remarks and discussions.

2 Field equations and solution

The Universe is initially considered to be homogeneous and isotropic, as described by the FLRW metric, which is expressed as follows [114]:

$$ds^2 = -dt^2 + a^2(t)\left[dr^2 + r^2(d\theta^2 + \sin^2\theta\, d\phi^2)\right], \tag{6}$$

where $a(t)$ represents the cosmic scale factor of the Universe. The Einstein field equations, incorporating a time-dependent cosmological constant term, are represented as:

$$R_{\mu\nu} - \frac{1}{2}g_{\mu\nu}R = 8\pi G\left(T_{\mu\nu} + g_{\mu\nu}\Lambda\right) = \tilde{T}_{\mu\nu}, \tag{7}$$

where $R = g^{\mu\nu}R_{\mu\nu}$ is the Ricci scalar, G denotes the Newtonian gravitational constant, and $T_{\mu\nu}$ is the energy-momentum tensor of matter. It is important to note that geometric units are utilized where $8\pi G = c = 1$.

In the concordance model $\nabla_\mu \tilde{T}^{\mu\nu} = 0$ i.e, the energy density of each fluid component is independently conserved [74]:

$$\dot{\rho}_i + 3H(1+\omega_i)\rho_i = 0, \tag{8}$$

where $i = (r, b, c, d)$ represents radiation, baryons, cold dark matter (CDM), and DE.

This research investigates a cosmological framework in which the Universe is understood to consist of two main elements: dark energy and matter. In this context, bulk viscous matter is regarded as DM, while vacuum energy density is considered as DE. In scenarios where an interaction between DM and DE occurs, the stress-energy tensors associated with DM and DE are not conserved independently; however, the overall stress-energy tensor remains conserved. This is articulated from (7) as follows [115]:

$$\nabla_\mu \tilde{T}^{\mu\nu}_m = +Qu^\nu_m/a \tag{9a}$$

$$\nabla_\mu \tilde{T}^{\mu\nu}_\Lambda = -Qu^\nu_m/a \tag{9b}$$

where the coefficient Q signifies the interaction between the two sectors, u^ν_m denotes the four-velocity of dark matter, and a represents the time-dependent scale factor of the Universe. Consequently, from (9), the resulting evolution equations for the energy densities of DM and DE are as follows [69]:

$$\dot{\rho}_m + 3H(\rho_m + p_m) = -Q, \tag{10}$$

$$\dot{\rho}_\Lambda + 3H(\rho_\Lambda + p_\Lambda) = Q. \tag{11}$$

In these equations, the dot represents differentiation with respect to coordinate time, while H signifies the Hubble rate. Additionally, ρ_m denotes the energy density of dark matter, and ρ_Λ represents the energy density of the vacuum. The variables p_m and p_Λ correspond to the pressures associated with matter and vacuum energy, respectively, and Q indicates the amount of energy that is exchanged. Non-relativistic matter is treated with $p_m = 0$. When $Q > 0$, dark matter transfers energy to dark energy; conversely, when $Q < 0$, the energy transfer occurs in the opposite direction [73]. It is also noted that $p_\Lambda = -\rho_\Lambda$.

It is posited that the universe is composed of bulk viscous matter, exhibiting viscous pressure as defined by the non-causal Eckart theory. New pressure becomes $P_{\text{eff}} = p_m + \Pi$. Within the framework of viscous dynamics, the bulk viscous pressure Π for the viscous fluid was initially introduced by Eckart in 1940 [29], and is represented by the following equation:

$$\Pi = -3\zeta H, \tag{12}$$

In this equation, ζ denotes the bulk viscous coefficient, which arises in the viscous fluid that departs from local thermal equilibrium [67]. It is assumed that ζ is positive based on thermodynamic principles. In our analysis, we have consider the newly accepted form of ζ given in (1).

This study aims to investigate the cosmological dynamics of the Universe, focusing on the interactions involving the dark matter component, which incorporates dissipation through a bulk viscous coefficient, alongside a vacuum energy density characterized by a running coupling that depends on the Hubble parameter [116,117]. Allowing Λ to vary and integrating it into the energy-momentum tensor addresses several issues inherent in the conventional cosmological model, such as the singularity, horizon, monopole, and cosmological constant problems [17,44,118–120]. We have considered the form of VED as given in (4).

In this analysis, it is assumed that the interaction Q is influenced by the Hubble parameter and the densities of pressureless matter, in addition to dark energy given in (5).

The Friedmann equation are expressed as follows:

$$3H^2 = \rho_m + \rho_\Lambda. \tag{13}$$

Using Eqs. (1), (4), (5), (10), (11), (12) and (13) and we obtain the evolution of H

$$\dot{H}+\frac{3H^2(\alpha-3\zeta_0(\nu-1)+\zeta_1+\nu-1)}{2(\nu-1)} +\frac{3H_0^2(3\zeta_0-1)(\nu-\Omega_\Lambda)}{2(\nu-1)}=0. \tag{14}$$

In order to simplify our calculations, we have adopted the substitution $x=\log a$. With respect to the dimensional Hubble parameter, represented as $h=\frac{H}{H_0}$, we can rewrite Eq. (14)

$$\frac{dh^2}{dx}+\frac{3(\alpha-3\zeta_0(\nu-1)+\zeta_1+\nu-1)}{\nu-1}h^2 +\frac{3(3\zeta_0-1)(\nu-\Omega_\Lambda)}{\nu-1}=0. \tag{15}$$

The solution of the Eq. (14) in terms of scale factor is given by

$$h^2=\frac{1}{\alpha-3\zeta_0(\nu-1)+\zeta_1+\nu-1}\times\Big(3\zeta_0(\Omega_\Lambda-\nu) +\nu-\Omega_\Lambda+(\alpha-3\zeta_0(\Omega_\Lambda-1)+\zeta_1 +\Omega_\Lambda-1)a^{-\frac{3(\alpha+\zeta_1)}{\nu-1}+9\zeta_0-3}\Big), \tag{16}$$

and the evolution of the Hubble parameter in terms of redshift is

$$H=H_0\sqrt{A+B(1+z)^k}, \tag{17}$$

where

$$A=\frac{\nu-\Omega_\Lambda+3\zeta_0(-\nu+\Omega_\Lambda)}{-1+\alpha+\zeta_1-3\zeta_0(-1+\nu)+\nu}, \tag{18a}$$

$$B=\frac{-1+\alpha+\zeta_1-3\zeta_0(-1+\Omega_\Lambda)+\Omega_\Lambda}{-1+\alpha+\zeta_1-3\zeta_0(-1+\nu)+\nu}, \tag{18b}$$

$$k=\frac{3(-1+\alpha+\zeta_1-3\zeta_0(-1+\nu)+\nu)}{-1+\nu}. \tag{18c}$$

3 Data analysis

To estimate the parameter values present in the expression of $H(z)$ in Eq. (17) for our proposed model, we concentrate on evidence pertinent to the universe's expansion history, particularly the distance-redshift relationship. In our model, we have 6 parameters, which are H_0, ν, α, ζ_0, ζ_1 and Ω_Λ. We utilize a range of observational data and methodologies to constrain the model parameters for both the ΛCDM and our proposed model. This includes data from the *Pantheon* dataset and *Cosmic Chronometer*. Utilizing the EMCEE Python module [107], we apply the MCMC statistical technique to explore the parameter space of our cosmological models and minimize the χ^2 function for both ΛCDM and interacting viscous models. MCMC is an influential statistical technique that enables a comprehensive and efficient estimation of uncertainties in model parameters using observational data [121,122]. In cosmology, MCMC algorithms play a crucial role in Bayesian inference, merging prior knowledge with observational data to create posterior probability distributions that depict the uncertainties associated with the parameters [123,124]. This thorough approach guarantees a reliable and precise estimation of the model parameters based on observational data.

3.1 *Pantheon* Supernovae data

Numerous compilations of Type Ia supernova (SNIa) data have been published over the years, including Union, Union2, Union2.1, JLA, *Pantheon*, and the latest, *Pantheon*+SH0ES [108,125–128]. For our analysis, we utilize the *Pantheon* SNIa data sets, which consist of 1048 Type Ia supernovae data covering redshift range $0.1\leq z\leq 2.3$ and offer comprehensive information for cosmological studies. The *Pantheon* sample is a collection of 279 $SNeIa$ discovered by the Pan-STARRS1 (PS1) Medium Deep Survey [129], the distance estimates from the Sloan Digital Sky Survey (SDSS) [130], Supernova Legacy Survey (SNLS) [131], from various low redshift and Hubble Space Telescope (HST) [132] samples. The connection between luminosity distance and redshift serves as a fundamental observational method for monitoring the evolution of the universe. The luminosity distance $D_L(z)$ can be expressed through the integral formula

$$D_L=c(1+z)\int_0^z\frac{dz'}{H(z')}, \tag{19}$$

where c is the speed of the light.

The theoretical apparent magnitude μ of standard candles is defined as [133]

$$\mu(z)=5\log_{10}\left(\frac{D_L}{\text{Mpc}}\right)+25. \tag{20}$$

In order to investigate the complete cosmological parameter space, we utilize the χ^2 statistics [134],

$$\chi^2_{Pan}=\Delta V^T C^{-1}\Delta V \tag{21}$$

where $\Delta V=\mu_{obs(z_i)}-\mu_{th(z)}$, represents the discrepancy between the apparent magnitudes of observed Type Ia supernovae at redshift z_i and those predicted theoretically. In this context, μ_{obs} is calculated using the formula $\mu_{obs}=m_B-\mathcal{M}$. Here, m_B refers to the observed peak magnitude in the B band's rest frame, while $\mathcal{M}$ denotes the absolute B-band magnitude of a reference SNe Ia, which can vary between -20 and -18. Here the total covariance matrix C is expressed as $C=D_s+C_s$, where, D_s represents the diagonal matrix, while C_s accounts for both statistical and systematic uncertainties.

3.2 Cosmic chronometer (CC)

The Hubble parameter is regarded as one of the most significant cosmological parameters by both theoretical and observational cosmologists, as it is integral to the study of the universe's evolution [135]. Measurements of the Hubble parameter are obtained from early-type galaxies that exhibit passive evolution, with their differential ages estimated along the line of sight [136,137]. In this analysis, we utilize a dataset of 31 CC data points [138], which spans a redshift range of 0.07 to 2.41. We compare the theoretical predictions of each model with the observational data using the chi-square function, defined as follows:

$$\chi^2_{CC} = \sum_{i=1}^{N} \frac{(H_{\rm th}(z_i, H_0, \nu, \alpha, \zeta_0, \zeta_1, \Omega_\Lambda) - H_{\rm obs}(z_i))^2}{\sigma^2_H(z_i)} \tag{22}$$

where $H_{\rm obs}$ refers to the observed values, $H_{\rm th}$ represents the theoretical values and σ^2_H signifies the observational errors associated with the measured values.

3.3 CC+*Pantheon*

The analysis involved the use of the combined cosmic chronometer and *Pantheon* dataset to estimate the values of the model parameters. The chi-squared function for the Hubble and *Pantheon* datasets is formulated as

$$\chi^2_{total} = \chi^2_{Pan} + \chi^2_{CC} \tag{23}$$

3.4 Statistical analysis and model comparision

This section focuses on the reduced chi-squared value and model selection criteria to evaluate the compatibility of the proposed model. The reduced chi-squared value [139] is defined as

$$\chi^2_{red} = \frac{\chi^2_{min}}{\mathcal{N} - n}, \tag{24}$$

where $\mathcal{N}$ represents the total number of observational data points, and n denotes the number of parameters. A reduced chi-squared value (χ^2_{red}) of less than 1 indicates an optimal fit with the data.

It is essential to conduct a statistical analysis using the Akaike Information Criterion (AIC) [140] and the Bayesian Information Criterion (BIC) [141]. These criteria are crucial for comparing models with varying degrees of freedom. The AIC, based on information theory, serves as an asymptotically unbiased estimator of Kullback–Leibler information. Assuming Gaussian errors, the AIC can be calculated using the formula provided [116,142]

$$\text{AIC} = \chi^2_{min} + 2n + \frac{2n(n+1)}{\mathcal{N} - n - 1} \tag{25}$$

For a large number of data points, it simplifies to AIC $= \chi^2_{min} + 2n$. The process of maximizing the likelihood function is directly related to minimizing the χ^2 statistic. The Bayesian Information Criterion (BIC) serves as an estimator of Bayesian evidence, as referenced by [141,143]:

$$\text{BIC} = \chi^2_{min} + n\ln(\mathcal{N}) \tag{26}$$

For enhanced analysis and comparison, the ΛCDM model is selected as a benchmark. The ΔAIC is defined as follows:

$$\Delta\text{AIC} = \text{AIC}_{\rm Model} - \text{AIC}_{\Lambda\rm CDM}. \tag{27}$$

Specifically, employing the Jeffreys scale [144], the condition $\Delta\text{AIC} \leq 2$ implies statistical compatibility of the model at hand with the reference model. A range of $4 < \Delta\text{AIC} < 7$ indicates a moderate level of disagreement between the two models. Finally, when $\Delta\text{AIC} \geq 10$, it reflects a significant degree of tension between the models, as noted by [145]. Similarly, if ΔBIC is below 2, it signifies strong support for the proposed theoretical model, whereas a range of $2 < \Delta\text{BIC} < 6$ indicates moderate support.

3.5 Observational constraints

To achieve optimal model parameters, we utilized the publicly available Cosmo Hammer (EMCEE) Python package to implement the MCMC method [146]. In this approach, the posterior distributions are derived from prior distributions and likelihood functions, with the likelihood expressed as follows:

$$L \propto \exp\left(-\frac{\chi^2}{2}\right). \tag{28}$$

We have analyzed data from CC and SNe Ia *Pantheon* supernovae, as well as their combination, to estimate the best-fit parameter values (H_0, ν, α, ζ_0, ζ_1, Ω_Λ). We conducted the MCMC Bayesian statistical computations, initiating with 1500 steps to stabilize the estimations during the burn-in phase, followed by 5000 MCMC steps utilizing 600 walkers. Flat priors were applied in all cases, defined as: $H \in [60, 90]$, $\nu \in [0, 0.1]$, $\alpha \in [-0.1, 0.1]$, $\zeta_0 \in [0, 0.1]$, $\zeta_1 \in [0, 0.1]$, $\Omega_\Lambda \in [0.6, 1]$. The estimated parameters for the ΛCDM model and the model under investigation, at a confidence level of 68.3%, are summarized in Table 1. Additionally, Fig. 1 depicts the two-dimensional posterior contours and the one-dimensional posterior distribution for the best-fit parameter values, including the 1σ and 2σ confidence regions derived from the dataset for our model.

We have also computed the values of ΔAIC and ΔBIC in relation to the ΛCDM model. The AIC penalizes models that have an excessive number of parameters, even if they yield a superior fit to the data. Therefore, a model with a lower AIC is favored over one with a higher AIC, as long as the difference in AIC is sufficiently significant [147]. The ΔAIC

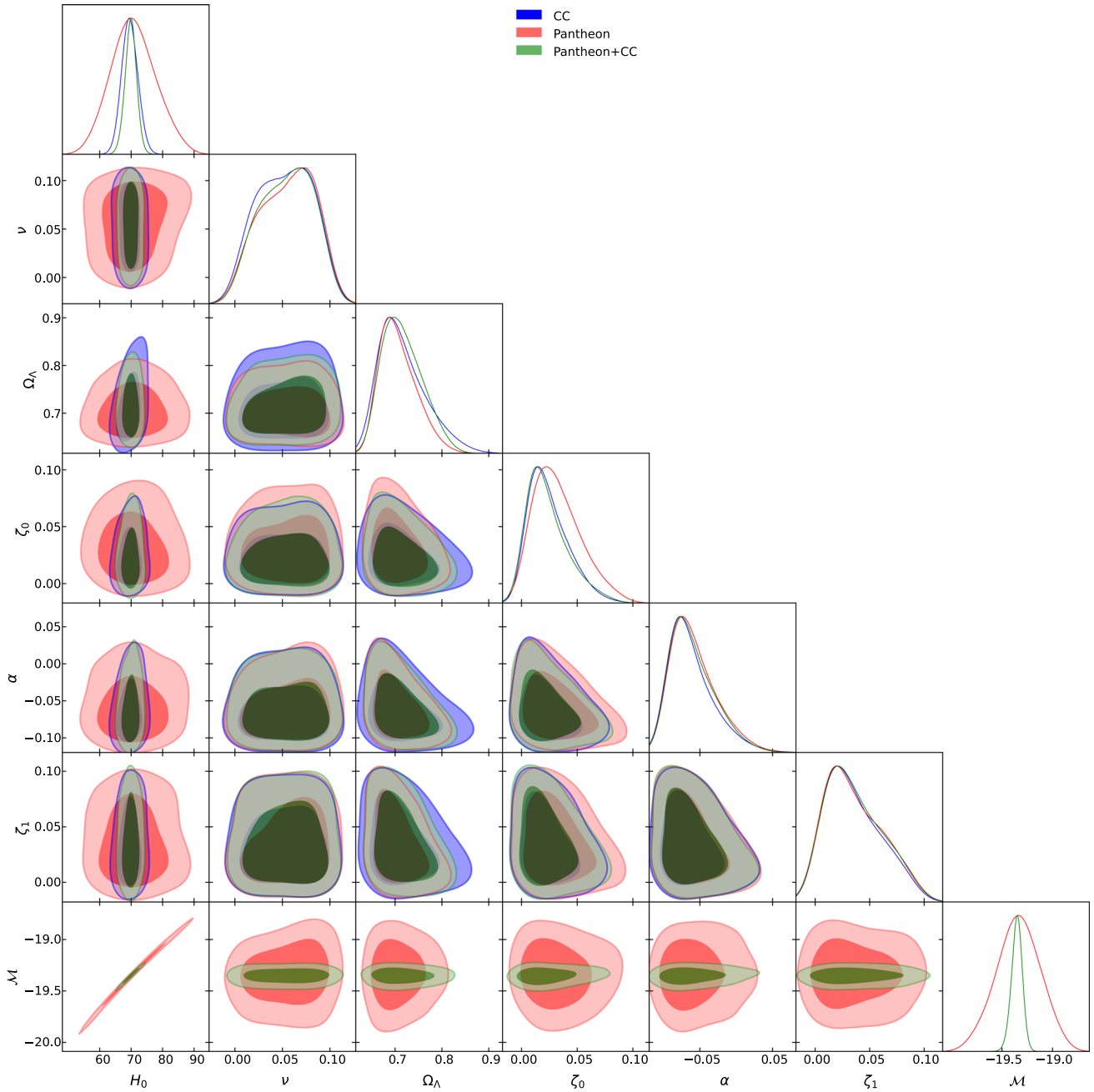

Fig. 1 The contour plots for the model parameters ν, Ω_Λ, ζ_0, α, ζ_1 and $\mathcal{M}$ with $1-\sigma$ and $2-\sigma$ confidence limits. It includes the best-fit values of the model parameters obtained from the CC, *Pantheon* and *Pantheon*+CC

values for CC and pantheon data indicate strong support for the proposed model and moderate support for the scenario where a joint analysis of Pantheon+CC is conducted as shown in Table 1. Conversely, it is commonly understood that a high ΔBIC value can be counterbalanced by a large number of parameters, except in the case of CC data where $\Delta BIC = 3.72$. However, the fact that χ^2_{red} is below 1 suggests that our proposed model fits the observational data well.

Figure 2a illustrates the evolution of the Hubble parameter for the Model and ΛCDM models, using the best predicted parameter values from the combined dataset, and compares these with the $H(z)$ data points. Moreover, Fig. 2b compares the evolution of the apparent magnitude μ of supernovae for both models with the *Pantheon* data points. The model's predictions are in close agreement with the observed values, suggesting its capability in accurately describing the cosmological phenomena related to the distance modulus.

Table 1 Best-fit of the model parameters. Statistical comparison of ΛCDM and the proposed model using χ^2, reduced χ^2, AIC, and BIC values. The ΛCDM model is taken as the reference for computing ΔAIC and ΔBIC

	CC		Pantheon		*Pantheon*+CC	
	ΛCDM	Model	ΛCDM	Model	ΛCDM	Model
H_0	70.69 ± 1.43	$69.75^{+2.15}_{-2.61}$	70 ± 0.020	$70.27^{+6.45}_{-5.49}$	$69.37^{+1.74}_{-1.75}$	$70^{+1.3}_{-1.6}$
ν	–	$0.051^{+0.034}_{-0.034}$	–	$0.056^{+0.031}_{-0.038}$	–	$0.056^{+0.030}_{-0.036}$
α	–	$-0.068^{+0.043}_{-0.020}$	–	$-0.067^{+0.038}_{-0.024}$	–	$-0.067^{+0.040}_{-0.024}$
ζ_0	–	$0.020^{+0.024}_{-0.014}$	–	$0.029^{+0.028}_{-0.020}$	–	$0.019^{+0.023}_{-0.014}$
ζ_1	–	$0.027^{+0.033}_{-0.020}$	–	$0.029^{+0.037}_{-0.021}$	–	$0.030^{+0.036}_{-0.047}$
Ω_m	0.256 ± 0.21	–	0.285 ± 0.20	–	$0.30^{+0.016}_{-0.015}$	–
Ω_Λ	–	$0.703^{+0.059}_{-0.0039}$	–	$0.697^{+0.048}_{-0.033}$	–	$0.708^{+0.052}_{-0.039}$
$\mathcal{M}$	–	–	–	$-19.34^{+0.19}_{-0.17}$	$-19.36^{+0.052}_{-0.054}$	$-19.34^{+0.039}_{-0.047}$
χ^2	23.61	13.59	1035.67	1026.76	1043.46	1040.44
χ^2_{red}	0.57	0.54	0.99	0.98	0.96	0.97
AIC	28.03	29.09	1041.69	1040.87	1049.48	1054.54
BIC	30.47	34.19	1056.53	1075.44	1064.41	1089.33
ΔAIC	–	1.06	–	−0.82	–	5.06
ΔBIC	–	3.72	–	18.91	–	24.92

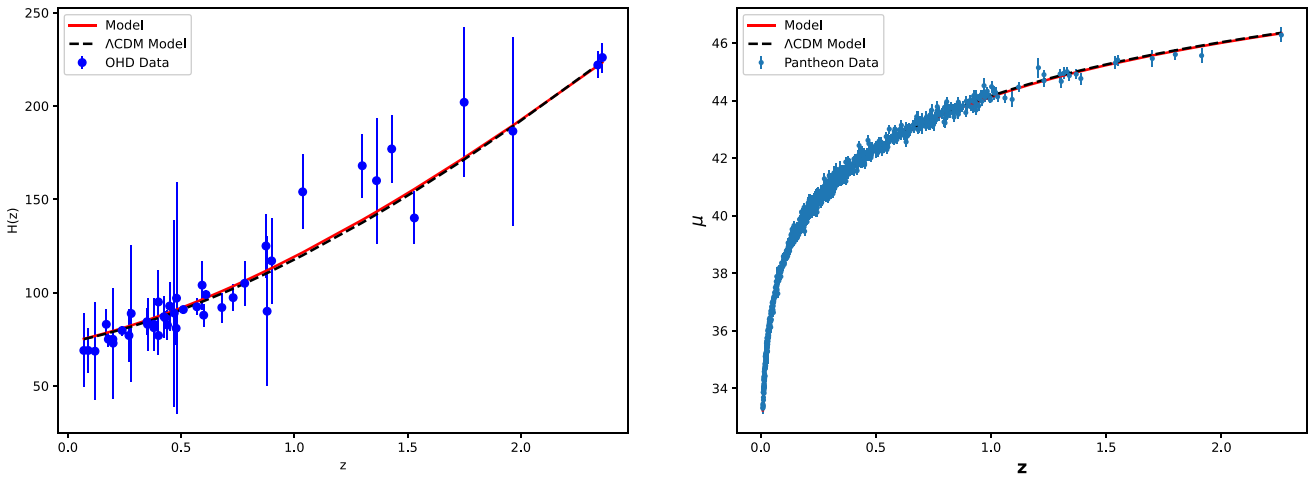

(a) (b)

Fig. 2 **a** The theoretical curve of the Hubble function $H(z)$ for Model (red) and ΛCDM (black) with $\Omega_{m_0} = 0.3, \Omega_{\Lambda_0} = 0.7$. Blue dots represent 43 $H(z)$ datasets. **b** The theoretical curve of the distance modulus $\mu(z)$ for Model (red) and ΛCDM (black) with the same parameters. Blue dots represent 1048 *Pantheon* datasets

4 Evolutionary behaviour of cosmological parameters

In this section, we examine the evolutionary characteristics of several fundamental cosmological parameters. These parameters encompass the deceleration parameter, the equation of state parameter (EoS), statefinder pairs, and the Om diagnostic. Through the analysis of these parameters, we can investigate the properties of dark energy, evaluate various cosmological models, and consider the consequences for the Universe's history and future dynamics. Here we also computed cosmological parameters using best-fit values of the model parameters and presented in Table 2.

4.1 Evolution of the Hubble parameter and Hubble tension

The evolution of the Hubble parameter in relation to redshift is presented in (17), and the corresponding graph is illustrated in Fig. 3.

Table 2 Best-fit values of cosmological parameters for different datasets

Param	CC	*Pantheon*	*Pantheon*+CC
q_0	$-0.494^{+0.173}_{-0.244}$	$-0.500^{+0.174}_{-0.234}$	$-0.504^{+0.175}_{-0.235}$
ω_{eff_0}	$-0.663^{+0.115}_{-0.163}$	$-0.667^{+0.116}_{-0.156}$	$-0.669^{+0.117}_{-0.157}$
r_0	$0.974^{+0.176}_{-0.189}$	$0.930^{+0.199}_{-0.182}$	$0.973^{+0.179}_{-0.181}$
s_0	$0.009^{+0.058}_{-0.070}$	$0.023^{+0.053}_{-0.075}$	$0.009^{+0.055}_{-0.070}$
z_{t_0}	$0.604^{+1.366}_{-0.318}$	$0.669^{+1.748}_{-0.371}$	$0.622^{+1.334}_{-0.330}$
Age (Gyr)	$13.240^{+1.030}_{-0.530}$	$13.480^{+1.270}_{-0.780}$	$13.280^{+0.980}_{-0.530}$

The illustration shows that as the high redshift $z \to \infty$, the Hubble parameter H tends towards infinity. This suggests that the universe's density also reaches infinity at this juncture, emphasizing the Big-Bang singularity during the universe's initial phase. Conversely, as z progresses towards the future, the Hubble parameter diminishes. The current value of the Hubble parameter is presented in Table 2.

This model also minimizes the so called Hubble tension. The Hubble tension denotes the significant difference between the Hubble constant H_0 values derived from early-universe observations and those obtained from local, late-universe measurements. From CMB perspective, Bennett et al. [148] reported a value of $H_0 = 70.00 \pm 0.20$ km/s/Mpc based on WMAP's nine-year data. The Planck satellite's observations of the cosmic microwave background (CMB), under the assumption of standard ΛCDM cosmology, yield a value of $H_0 = 67.4 \pm 0.5$ km/s/Mpc [149]. Earlier releases of Planck data produced similar findings: $H_0 = 67.40 \pm 1.40$ km/s/Mpc in 2013 [150], which was refined to 67.40 ± 0.50 km/s/Mpc in the final release. When combining Planck data with lensing and BAO, H_0 is further constrained to 67.36 ± 0.54 km/s/Mpc and 67.66 ± 0.42 km/s/Mpc [151], respectively. In contrast, local measurements-derived from the cosmic distance ladder utilizing Cepheid variables and Type Ia supernovae-consistently yield higher values. Initial estimates from HST indicated $H_0 = 72 \pm 8$ km/s/Mpc [152], which was later refined to 74.3 ± 2.1 km/s/Mpc [153] through improved distance calibration. The latest result from the SH0ES collaboration is $H_0 = 73.04 \pm 1.04$ km/s/Mpc [154], with various reanalyses employing different statistical methods and datasets confirming the high value. This increasing discrepancy, now exceeding the 5σ threshold, has prompted extensive investigation [155]. Nevertheless, despite numerous studies, no convincing explanation has emerged. Reanalyses of both Planck and HST data indicate that systematic errors are unlikely to explain the observed tension, suggesting instead the potential for new physics beyond the ΛCDM model.

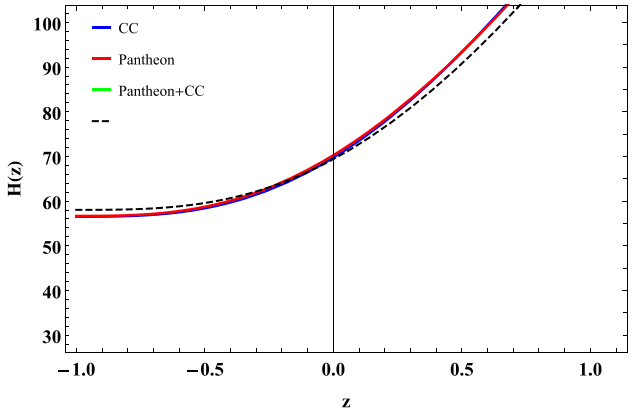

Fig. 3 Behaviour of the Hubble parameter H with respect to redshift z from (17) for the best-fit of the model parameter

Our proposed model results in $H_0 = 69.75^{+2.15}_{-2.61}$ km s^{-1} Mpc^{-1} for CC, $70.27^{+6.45}_{-5.49}$ km s^{-1} Mpc^{-1} for Pantheon, and $70^{+1.3}_{-1.6}$ km s^{-1} Mpc^{-1} for both Pantheon and CC. It is important to highlight that Riess et al. [154] report a value of H_0 as 73.04 ± 1.04 km s^{-1} Mpc^{-1}, known as R21, while the Planck Collaboration [149] predicts H_0 =67.4 ± 0.5 kms^{-1} Mpc^{-1} at a 5σ confidence level. Our derived value is within this range, indicating a tension of 0.97σ and 1.27σ with the findings from both Planck and R21 for CC, and 0.48σ and 0.46σ for Pantheon, with 1.70σ and 1.70σ for Pantheon+CC.

4.2 Deceleration parameter

The deceleration parameter is a crucial parameter for understanding the dynamics and evolution of the cosmos. It is mathematically represented by the equation [156]

$$q = -\frac{\ddot{a}a}{a^2} = -1 - \frac{\dot{H}}{H^2}. \tag{29}$$

A positive value of the deceleration parameter ($q > 0$) suggests that the Universe is experiencing deceleration, whereas a negative value ($q < 0$) indicates that the expansion of the Universe is accelerating.

Putting Eqs. (17) and (18) into Eq. (29), we obtain the deceleration parameter q for our model as:

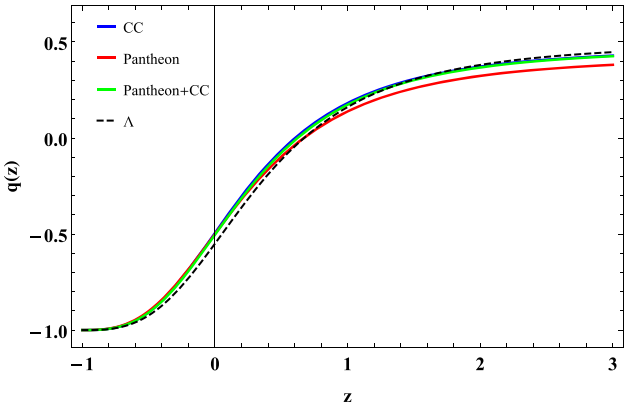

Fig. 4 Behaviour of the deceleration parameter q with respect to redshift z from (30) for the best-fit of the model parameter

made by several researchers employing different methodologies [159,160]. This value is also comparable to the transition redshift, $z_t = 0.50 - 0.73$ obtained for the ΛCDM model [161,162].

4.3 Effective equation of state (EoS)

The behavior of the effective equation of state parameter signifies the phase of accelerating expansion in the universe. This parameter is characterized by the ratio of pressure to energy density, expressed as

$$\omega_{\text{eff}} = \frac{P_{\text{eff}}}{\rho_m + \rho_\Lambda}. \tag{31}$$

$$q(z) = -1 - \frac{3(1+z)^{\left(3-9\zeta_0+\frac{3(\alpha+\zeta_1)}{-1+\nu}\right)}(-1+\alpha+\zeta_1-3\zeta_0(-1+\nu)+\nu)(-1+\alpha+\zeta_1-3\zeta_0(-1+\Omega_\Lambda)+\Omega_\Lambda)}{2(-1+\nu)(-\nu+3\zeta_0(\nu-\Omega_\Lambda)+(1+z)^{\left(3-9\zeta_0+\frac{3(\alpha+\zeta_1)}{-1+\nu}\right)}(1-\alpha-\zeta_1+3\zeta_0(-1+\Omega_\Lambda)-\Omega_\Lambda)+\Omega_\Lambda)}. \tag{30}$$

We calculate the deceleration parameter for the present epoch ($z = 0$) using the best-fit values of the model parameters derived from the $H(z)$ data, *Pantheon* sample, and *Pantheon*+CC for the model. This results in $q_0 = -0.494^{+0.173}_{-0.244}$, $q_0 = -0.500^{+0.174}_{-0.234}$, and $-0.504^{+0.175}_{-0.235}$, respectively. The obtained value of q_0 closely aligns with the WMAP measurement of $q_0 = -0.60$ [157]. In Fig. 4, the relationship between q and redshift z is illustrated using the best-fit model parameters. This figure effectively showcases the evolutionary dynamics of the universe, particularly the transition from deceleration to acceleration. As $z \to -1$, the universe is expected to approach thermodynamic equilibrium in the distant future ($q = -1$) [158], as depicted in the diagram.

The redshift at which the transition from the decelerated phase to the accelerated phase occurs has been determined, yielding values of $z_{t0} = 0.604^{+1.366}_{-0.318}$ for CC, $z_{t0} = 0.669^{+1.748}_{-0.371}$ for *Pantheon*, and $z_{t0} = 0.622^{+1.334}_{-0.330}$ for *Pantheon*+CC. These outcomes align with earlier discoveries

When the equation of state parameter takes on a value of $\omega < -\frac{1}{3}$, the universe transitions into the accelerating phase [163]. A value of $\omega < -1$ is linked to the phantom phase, while the range $-1 < \omega < -\frac{1}{3}$ corresponds to the quintessence phase [164].

Putting Eqs. (4), (13), (17), (18), (31) in Eq. (29), we obtained the EoS (ω_{eff}) for our model as

$$\begin{aligned}\omega_{\text{eff}} = {} & \frac{1}{(-1+\nu)\left((1+z)^{9\zeta_0+\frac{3}{-1+\nu}}(-1+3\zeta_0)(\nu-\Omega_\Lambda)-(1+z)^{\frac{3(\alpha+\zeta_1+\nu)}{-1+\nu}}(-1+\alpha+\zeta_1-3\zeta_0(-1+\Omega_\Lambda)+\Omega_\Lambda)\right)} \\ & \times\Big((1+z)^{9\zeta_0+\frac{3}{-1+\nu}}(1-3\zeta_0)(-1+\nu)(\nu-\Omega_\Lambda)-(1+z)^{\frac{3(\alpha+\zeta_1+\nu)}{-1+\nu}}(\alpha+\zeta_1-3\zeta_0(-1+\nu)) \\ & (-1+\alpha+\zeta_1-3\zeta_0(-1+\Omega_\Lambda)+\Omega_\Lambda)\Big).\end{aligned} \tag{32}$$

The present value of the equation of state parameter, based on the best-fit model parameters, is $\omega_{\text{eff}_0} = -0.663^{+0.115}_{-0.163}$ for CC data, $\omega_{\text{eff}_0} = -0.667^{+0.116}_{-0.156}$ for *Pantheon* data, and $\omega_{\text{eff}_0} = -0.669^{+0.117}_{-0.157}$ for the combination of *Pantheon* and *CC* data. These values represent that the model in Quintessence phase. The evolution of the equation of state with redshift z for the current model is shown in Fig. 5. At $z \to -1$, Model converges with the ΛCDM model, where $\omega = -1$, indicating a transition to the de Sitter phase in the late-time universe.

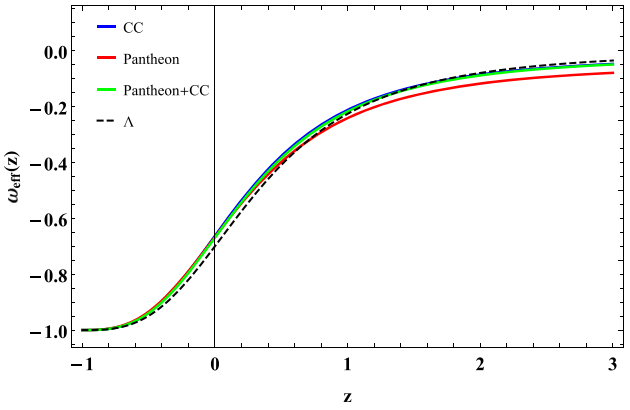

Fig. 5 Behaviour of the effective EoS $\omega_{\rm eff}$ with respect to redshift z from (32) for the best-fit of the model parameter

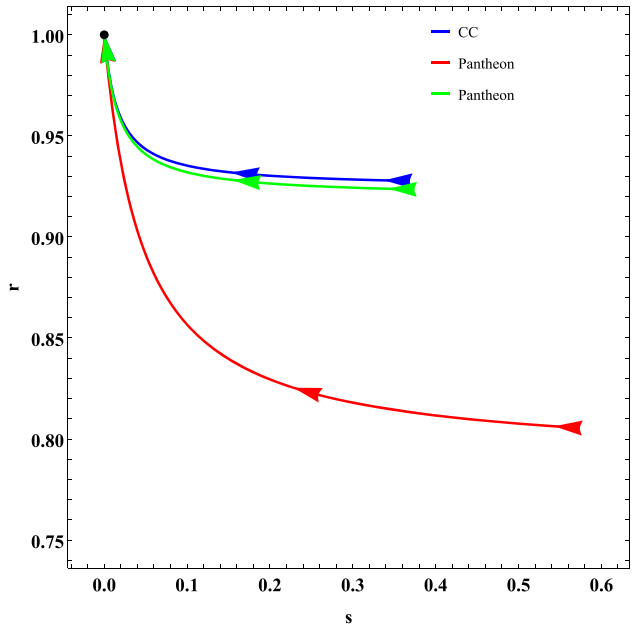

Fig. 6 The $\{r, s\}$ profile (34) and (35) for the best-fit of the model parameter. The black dot represents the ΛCDM point

4.4 Statefinder diagnostics

To distinguish a diverse array of dark energy models from established frameworks such as ΛCDM, SCDM, holographic dark energy, Chaplygin Gas, and Quintessence, statefinder diagnostics provide a robust geometrical approach, originally introduced by Sahni [165]. The statefinder parameters are defined as follows:

$$r = \frac{\dddot{a}}{aH^3}, \quad s = \frac{r-1}{3(q-\frac{1}{2})}. \tag{33}$$

In this context, a denotes the scale factor, H signifies the Hubble parameter, and q represents the deceleration parameter. The condition $(r < 1, s > 0)$ indicates the presence of quintessence dark energy, while the region defined by $(r > 1, s < 0)$ corresponds to the phantom scenario. Additionally, the point $(r = 1, s = 0)$ characterizes the conventional ΛCDM model [166,167]. Using Eqs. (17), (18) in Eq. (33) we get the following pairs for Model

The current values of the statefinder pairs, as derived from the best-fit values of the model parameters, are represented as $\{r_0, s_0\}$=$\{0.974^{+0.176}_{-0.189}, 0.009^{+0.058}_{-0.070}\}$ for the CC data, $\{r_0, s_0\}$=$\{0.930^{+0.199}_{-0.182}, 0.023^{+0.053}_{-0.075}\}$ for the *Pantheon* data, and $\{r_0, s_0\}$=$\{0.973^{+0.179}_{-0.181}, 0.009^{+0.055}_{-0.070}\}$ for the combined *Pantheon*+CC dataset. Thus, the existing current values of the statefinder parameters in the proposed model are indicative of quintessence-type behavior. The behavior of these statefinder parameters in the $s-r$ plane is illustrated in the accompanying figure. In Fig. 6, the fixed point (0, 1) represents the spatially flat ΛCDM model. The trajectory is non-linear and progresses in the negative direction of s

$$r = \frac{1}{2(-1+\nu)^2(-\nu+3\zeta_0(\nu-\Omega_\Lambda)+(1+z)^{3-9\zeta_0+\frac{3(\alpha+\zeta_1)}{-1+\nu}}(1-\alpha-\zeta_1+3\zeta_0(-1+\Omega_\Lambda)-\Omega_\Lambda)+\Omega_\Lambda)}$$
$$\Big(2(-1+3\zeta_0)(-1+\nu)^2(\nu-\Omega_\Lambda)-(1+z)^{3-9\zeta_0+\frac{3(\alpha+\zeta_1)}{-1+\nu}}(-1+3\alpha+3\zeta_1-9\zeta_0(-1+\nu)+\nu)$$
$$\times(-2+3\alpha+3\zeta_1-9\zeta_0(-1+\nu)+2\nu)(-1+\alpha+\zeta_1-3\zeta_0(-1+\Omega_\Lambda)+\Omega_\Lambda)\Big), \tag{34}$$

$$s = \frac{1}{(-1+3\zeta_0)(-1+\nu)^3(\nu-\Omega_\Lambda)+(1+z)^{3-9\zeta_0+\frac{3(\alpha+\zeta_1)}{-1+\nu}}(\alpha+\zeta_1-3\zeta_0(-1+\nu))(-1+\nu)^2(-1+\alpha+\zeta_1-3\zeta_0(-1+\Omega_\Lambda)+\Omega_\Lambda)}$$
$$\times\Big((1+z)^{3-9\zeta_0+\frac{3(\alpha+\zeta_1)}{-1+\nu}}(\alpha+\zeta_1-3\zeta_0(-1+\nu))(-1+\nu)\times(-1+\alpha+\zeta_1-3\zeta_0(-1+\nu)+\nu)$$
$$\times(-1+\alpha+\zeta_1-3\zeta_0(-1+\Omega_\Lambda)+\Omega_\Lambda)\Big). \tag{35}$$

and the positive direction of r. It is observed that the model resides within the quintessence region, defined by $r < 1$ and $s > 0$, and it is expected to converge towards ΛCDM in the future as shown in Fig. 6. The deviation from the ΛCDM point occurs because, within the ΛCDM framework, the Λ-term acts as dark energy, which remains constant, leading to an EoS of $\omega = -1$. In contrast, our model features a varying VED and also considers interactions between DM and DE. This results in a slower expansion compared to ΛCDM [168].

4.5 Om diagnostic

In addition to the statefinder diagnostic, Sahni et al. [169] introduced a novel diagnostic known as the Om(z) diagnostic. This diagnostic is advantageous as it relies solely on the first derivative of the scale factor, making it simpler to reconstruct than the statefinder parameters. For a universe that is spatially flat, the expression is defined as follows [170]:

$$Om(z) = \frac{H^2(z)/H_0^2 - 1}{(1+z)^3 - 1}. \tag{36}$$

Much like the statefinder diagnostic, the Om diagnostic serves as an effective tool for differentiating between various dark energy (DE) models based on the variations in slope. A negative slope of Om(z) suggests that dark energy exhibits quintessence-type behavior ($\omega > -1$), whereas a positive slope indicates phantom-type behavior ($\omega < -1$). A constant value of Om(z) is indicative of the cosmological constant (ΛCDM) model [171]. Substituting Eqs. (17), (18) into Eq. (36), $Om(z)$ takes the form:

$$Om(z) = \frac{\left(-1 + (1+z)^{\frac{3(-1+\alpha+\zeta_1-3\zeta_0(-1+\nu)+\nu)}{-1+\nu}}\right)}{z(3+3z+z^2)} \times \frac{(-1+\alpha+\zeta_1-3\zeta_0(-1+\Omega_\Lambda)+\Omega_\Lambda)}{(-1+\alpha+\zeta_1-3\zeta_0(-1+\nu)+\nu)}. \tag{37}$$

Figure 7 depicts the behavior of the $Om(z)$ parameter within the context of the proposed model. Throughout the range of estimated parameter values, the slope of the $Om(z)$ curve shows a continuous decrease. Thus, according to the Om diagnostic test, we can infer that our model demonstrates quintessence-like characteristics. It is clear from Fig. 7 that $Om(z)$ is constant (black dashed line) for the ΛCDM model. On the other hand, our model results a negative slope for the Om(z) diagnostic. This is because of time varying nature of VED with bulk viscosity. It is observed that when bulk viscosity is absent, the model exhibits a positive slope, indicating a panthon characteristic. In the absence of both bulk viscosity and the VED term, the model functions as a straightforward ΛCDM model.

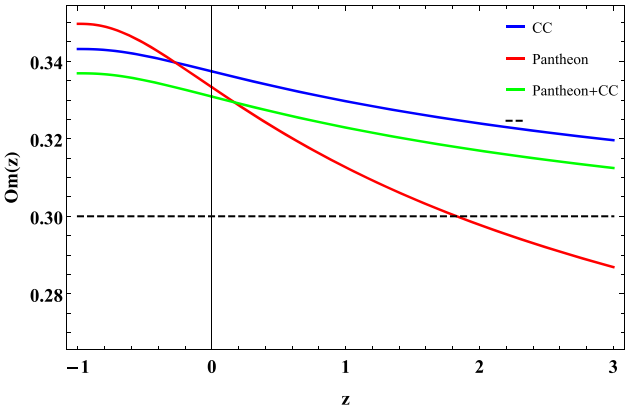

Fig. 7 Behaviour of the Om diagnostic Om with respect to redshift z from (37) for the best-fit of the model parameter

4.6 The age of the universe

Our previous analysis substantiates the occurrence of a Big Bang at the universe's origin, enabling a precise calculation of its age. We can identify the cosmic time t_{BB} that corresponds to the Big Bang event. Consequently, the interval from t_{BB} to the present time t_0 is defined as the age of the universe as

$$Age \equiv t_{BB} - t_0 = \int_0^\infty \frac{dz}{(1+z)H(z)}. \tag{38}$$

Utilizing the best-fit values of the model parameters derived from the CC data, *Pantheon* sample, and *Pantheon*+CC data, the current estimation of the universe's age is $13.240^{+1.030}_{-0.530}$ Gyr, $13.480^{+1.270}_{-0.780}$ Gyr, and $13.280^{+0.980}_{-0.530}$ Gyr, respectively. In contrast, age estimates from the oldest globular clusters and Planck yield 12.9 ± 2.9 Gyr and 13.79 Gyr, respectively [149,172]. Thus, our estimated age is below this range.

5 Entropy evolution and the second law of thermodynamics

According to the second law of thermodynamics, entropy is required to increase continuously, illustrating the irreversibility of the universe [173]. In this study, we aim to assess the accuracy of the generalized second law (GSL) of thermodynamics [174]. The GSL posits that the entropy linked to cosmic components-such as matter, radiation, and DE-within the Hubble horizon, along with the entropy of the Hubble horizon itself, consistently rises over time. It is expressed as

$$\frac{d}{dt}(S_m + S_\Lambda + S_h) \geq 0, \tag{39}$$

where S_m signifies the entropy linked to nonrelativistic matter, whereas S_Λ indicates the entropy contribution from dark

energy. In this framework, S_h refers to the horizon entropy [175] and is articulated as

$$S_h = \frac{Ak_B}{4l_p^2}. \tag{40}$$

In this context, k_B is recognized as the Boltzmann constant, $A = 4\pi H^2$ denotes the area of the Hubble horizon, and $l_p = \sqrt{\frac{\hbar G}{c^3}}$ is referred to as the Planck length. We can utilize a natural system of units where $\hbar = c = k_B = 8\pi G = 1$. Under these conditions, Eq. (40) simplifies to

$$S_h = \frac{8\pi^2}{H^2}. \tag{41}$$

It is evident that the vacuum energy density in the present model doesn't contribute to the entropy as $p_\Lambda = -\rho_\Lambda$. Following [176], we derive the entropy associated with non-relativistic matter

$$S_m = \frac{(\rho_m + P_{\text{total}})V}{T}. \tag{42}$$

Here, ρ_m signifies the matter density, and P_{total} refers to the pressure attributed to bulk viscous matter. The volume defined by the horizon is represented as $V = (\frac{4\pi}{3H^2})$. We assume that the system limited by the Hubble horizon is in equilibrium, which results in a uniform temperature distribution equal to that of the horizon [177]. Additionally, we assume that the temperature T related to both matter and DE is identical due to their mutual interaction. The Gibbons-Hawking temperature, given by $T = H/2\pi$, is an appropriate choice for the horizon temperature [178]. In this case, S_Λ is zero, as the vacuum energy density does not contribute to entropy, since $p_\Lambda = -\rho_\Lambda$. From (1), (12), (17), (41), and (42) we obtain the total entropy $S = S_m + S_h$ as

$$S = \frac{-8\pi^2}{H_0^2\left(Ba^{-k}+A\right)^2}\Big(A + a^{-k}B)(\zeta_1 + 3\zeta_0(-1+\nu) - \nu) - (-1+3\zeta_0)(\nu - \Omega_\Lambda)\Big), \tag{43}$$

where A, B, and k are given in (18). Figure 8 depicts the relationship between entropy and the scale factor, indicating that entropy tends to reach a maximum value as time advances. To further elucidate this observation, we calculate the first and second derivatives of entropy concerning the scale factor. In order to confirm the condition specified in Eq. (39) for this model, it is beneficial to transition from a time variable to a scale factor variable and assess the rate of change of entropy in relation to the scale factor.

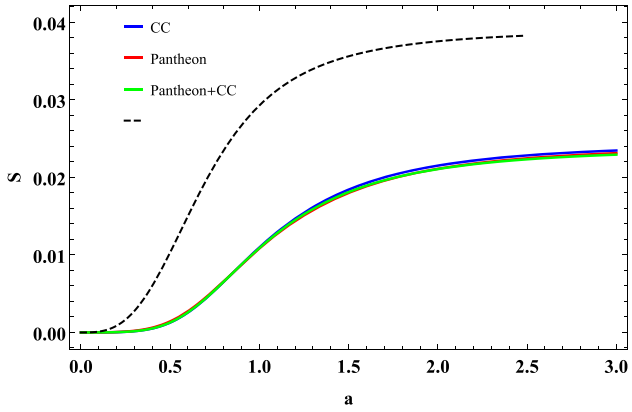

Fig. 8 Evolution of total entropy S vs scale factor a from (43) for best-estimated values of the model parameters

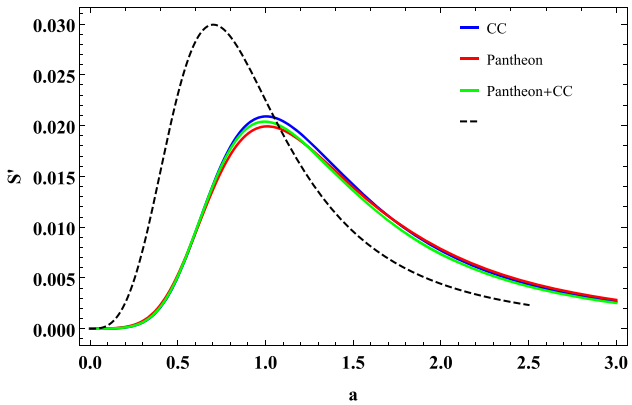

Fig. 9 Rate of entropy change S' vs scale factor a from (44) for best-estimated values of the model parameters and validity of GSL (in natural units)

$$S' = \frac{-8\pi^2 Bka^k}{H_0^2\left(Ba^{-k}+A\right)^3}\Big(B\left(\zeta_1 + 3\zeta_0(-1+\nu) - \nu\right) + a^k(A\left(\zeta_1 + 3\zeta_0(-1+\nu) - \nu\right) - 2(-1+3\zeta_0)(\nu - \Omega_\Lambda))\Big), \tag{44}$$

From Eq. (44), we derive that $S \geq 0$, which complies with GSL. As we near the asymptotic limit $a \to \infty$, $S \to 0$, indicating that the entropy reaches its maximum and implying that the final phase signifies an equilibrium state. These scenarios are clearly illustrated in Fig. 9.

To verify the maximization of horizon entropy, we analyze the second derivative concerning the scale factor

$$S'' = \frac{8\pi^2 Bka^{-3k-1}}{H_0^2\left(Ba^{-k}+A\right)^4}\Big(-B^2(-1+k)(\zeta_1 + 3\zeta_0(-1+\nu) - \nu) + a^{2k}A(1+k)$$

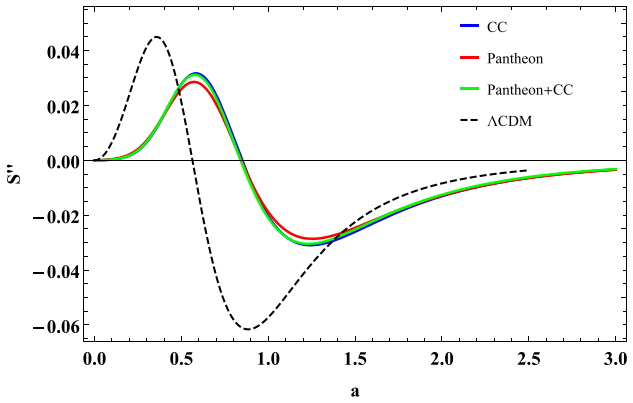

Fig. 10 Evolution of S'' vs scale factor a from (45) for best-estimated values of the model parameters

$$\begin{aligned}&(A\,(\zeta_1+3\zeta_0(-1+\nu)-\nu)-2(-1+3\zeta_0)(\nu-\Omega_\Lambda))\\&+2a^k B(A\,(\zeta_1+3\zeta_0(-1+\nu)-\nu)\\&+(-1+2k)(-1+3\zeta_0)(\nu-\Omega_\Lambda))\Big)\end{aligned}\tag{45}$$

Figure 10 illustrates that $S'' > 0$ during the initial stages of evolution, transitioning to $S'' < 0$ in the more recent past close to the transition redshift. Consequently, our model aligns with the principles of thermodynamics and supports the second law of thermodynamics.

6 Dynamical systems analysis

The theoretical framework of any proposed cosmological model must incorporate elements that elucidate the sequence Inflation → Radiation → Matter → Dark Energy [112]. Inflation is required to be characterized as an unstable point to facilitate the Universe's transition from this phase [179]. This section employs the principles of dynamical systems theory to examine the long-term qualitative behavior of the system and to explore potential cosmological scenarios [180,181] derived from the analysis of the model equation, excluding radiation. When the cosmological model includes multiple cosmic components, solving the model equation can often be complex. Nevertheless, the methods utilized in dynamical system analysis allow for the circumvention of the nonlinear aspects of the equation, enabling a straightforward description of the global dynamics without necessitating knowledge of the initial conditions [182,183]. The analysis commences with the computation of the eigenvalues of the linearized system at critical points, which are pivotal for the cosmological model. The characteristics of these critical points, as revealed through phase plane analysis, can provide insights into different cosmological epochs [184]. To facilitate a universal analysis, the formulation of autonomous differential equations for the model equation using appropriate dimensionless variables is prioritized. The initial step involves defining the dimensionless variables that span the phase space of the system, allowing for the rewriting of their dynamics in the form of an autonomous system. For qualitative analysis, the following dimensionless variables are chosen:

$$y_1 = \frac{\rho_m}{3H^2},\tag{46a}$$

$$y_2 = \frac{\rho_\Lambda}{3H^2},\tag{46b}$$

$$y_3 = \frac{Q}{3H^3},\tag{46c}$$

which are normalized over the Hubble scale. Consequently, the Friedmann constraint assumes the usual form

$$y_1 + y_2 = 1.\tag{47}$$

Utilizing the Friedmann equations (13), conservation equation for matter (10), (11) with these variables (46), the aforementioned cosmological equations can be converted into the following autonomous system as

$$\begin{aligned}y_1' = 3\Big[&\zeta_1 + y_1(\alpha+3\zeta_0-\zeta_1-1)\\&+(1-3\zeta_0)y_1(1-y_2)+\alpha y_2\Big] = f(y_1,y_2),\end{aligned}\tag{48a}$$

$$y_2' = -3\left[y_1\left(\alpha+(3\zeta_0-1)y_2\right)+y_2(\alpha+\zeta_1)\right] = g(y_1,y_2),\tag{48b}$$

where the prime denotes the derivative with respect to $N = \ln a$.

The critical points (y_{1_0}, y_{2_0}) of the above autonomous equations Eqs. (48a) and (48b) can be obtained by equating $y_1' = 0$ and $y_2' = 0$. The stability of the universe in the vicinity of the critical points are obtained by considering a linear perturbation around the critical point, $y_1 \to y_{1_0} + \delta y_1$, $y_2 \to y_{2_0} + \delta y_2$ which satisfy the following matrix equation,

$$\begin{bmatrix}\delta y_1'\\ \delta y_2'\end{bmatrix} = \begin{bmatrix}\left(\frac{\partial f}{\partial y_1}\right)_0 & \left(\frac{\partial f}{\partial y_2}\right)_0\\ \left(\frac{\partial g}{\partial y_1}\right)_0 & \left(\frac{\partial g}{\partial y_2}\right)_0\end{bmatrix}\begin{bmatrix}\delta y_1\\ \delta y_2\end{bmatrix}\tag{49}$$

Here, the suffix 0 signifies the value calculated at the critical point $(y_{1_0}\, y_{2_0})$. The Jacobian matrix is structured as a 2×2 matrix. The nature of the critical points is influenced by the signs of the eigenvalues of the `Jacobian matrix`. The `Jacobian matrix` for the model is

$$J = \begin{bmatrix}3\Big(\alpha+3\zeta_0-\zeta_1 & 3\alpha\big|_0\\ \quad +2(1-3\zeta_0)y_1-1\Big)\big|_0 & \\ -3\Big(\alpha+(3\zeta_0-1)y_2\Big)\big|_0 & -3\Big(\alpha+\zeta_1\\ & \quad +(3\zeta_0-1)y_1\Big)\big|_0\end{bmatrix}\tag{50}$$

From the perspective of dynamical system analysis, it is crucial to note that a critical point is unstable if all eigenvalues possess positive real parts, whereas it is stable if all eigenvalues have negative real parts. If at least one eigenvalue has a real part with a different sign, the critical point is categorized as a saddle point [185].

To analyze the behavior linked to the critical points of the autonomous system (48a)–(48b), we now present the deceleration parameter expressed in terms of dimensionless variables. According to Eq. (29), the deceleration parameter q, in relation to u and v, can be formulated as

$$q = \frac{3(\alpha + \zeta_1 + 3\zeta_0 y_1 + y_2 - 1)}{2(v-1)} - 1. \tag{51}$$

6.1 Critical points and stability

Equating (48a) and (48b) to zero has led us to identify two critical points. The characteristics of these critical points are analyzed below by determining the eigenvalues of the `Jacobian matrix` for the two critical points, utilizing the standard criteria for linear stability assessment.

6.1.1 Critical point A

The first critical point coordinates are $A\left(y_{1_{10}}, y_{2_{10}}\right)$, where $y_{1_{10}} = \left(-\frac{1-3\zeta_0+\zeta_1+\sqrt{4\alpha(-1+3\zeta_0)+(-1+3\zeta_0+\zeta_1)^2}}{-2+6\zeta_0}\right)$, and $y_{2_{10}} = \left(\frac{-1+3\zeta_0+\zeta_1+\sqrt{4\alpha(-1+3\zeta_0)+(-1+3\zeta_0+\zeta_1)^2}}{-2+6\zeta_0}\right)$.

By employing the optimal parameter values obtained from the *CC*, *Pantheon* sample, and *Pantheon*+CC data, we identify the critical points as $(1.069, -0.069)$, $(1.070, -0.070)$, and $(1.068, -0.068)$, respectively. At this identified critical point, the values of $y_{1c} \approx 0$ and $y_{2c} \approx 0$ indicate that matter predominates over dark energy, signifying a phase characterized by deceleration. From (51), the deceleration parameters are recorded as $q = 0.467$, $q = 0.423$, and $q = 0.466$, corresponding to the *CC*, *Pantheon* sample, and *Pantheon*+CC data, respectively. This approximate value of the deceleration parameter, 0.5, implies that we inhabit a universe primarily influenced by matter. The eigenvalues associated with the critical point are $(-0.081, 3.131)$, $(-0.087, 3.131)$, and $(-0.09, 3.126)$. Given that both eigenvalues exhibit both positive and negative values, this critical point is categorized as a saddle. It is well accepted that cold dark matter acts as the main element during the matter-dominated epoch at redshift $1 \leq z \leq 10^3$, and therefore, it is fundamental to structure formation in the universe during this time.

6.1.2 Critical point B

The second critical point coordinates are $B\left(y_{1_{20}}, y_{2_{20}}\right)$, where $y_{1_{20}} = \left(\frac{-1+3\zeta_0-\zeta_1+\sqrt{4\alpha(-1+3\zeta_0)+(-1+3\zeta_0+\zeta_1)^2}}{-2+6\zeta_0}\right)$, and $y_{2_{20}} = \left(\frac{-1+3\zeta_0+\zeta_1-\sqrt{4\alpha(-1+3\zeta_0)+(-1+3\zeta_0+\zeta_1)^2}}{-2+6\zeta_0}\right)$.

Utilizing the best parameter values derived from the *CC*, *Pantheon* dataset, and *Pantheon*+CC data, the critical points found are $(-0.040, 1.040)$, $(-0.038, 1.038)$, and $(-0.036, 1.036)$, respectively. These key values suggest that when y_{2c} approaches 1, the supremacy of dark energy surpasses that of matter, resulting in an accelerated phase. The deceleration parameter has a value of $q = -1$, and cosmic evolution near these critical points indicates a de-Sitter expansion with $\omega = -1$. The eigenvalues corresponding to these critical points are $(-0.081, -3.131)$, $(-0.087, -3.038)$, and $(-0.09, -3.126)$. Since eigenvalues consist of both negatives, this critical point is a stable future attractor.

In the framework of ΛCDM cosmology, the cosmological equations can be reformulated into an autonomous format: $\Omega_m = 3(\Omega_m - 1)\Omega_m$. This system presents two critical points, which are defined by $\Omega_m = 1$ and $\Omega_m = 0$. It is clear that the former is unstable, while the latter is stable [186]. In our examination, Point B represents an alternative solution compared to the ΛCDM scenario, where instead of the conventional cosmological constant-dominated solution characterized by $y_{1_{20}} = 0$, $y_{2_{20}} = 1$, and $\omega_{eff} = -1$, we now identify a scaling solution that depends on the interacting parameter α. It is important to note that a potential coupling between radiation and dark energy could significantly influence the dynamics of the early Universe [187]. The complete thermal history of the Universe encompasses the radiation-dominated era, transitions through the standard matter-dominated era, and extends to later times when the dark energy component dominates the total energy density and pressure of the Universe. In our analysis, we have not taken into account the radiation component, thus the Universe begins from a saddle matter-dominated state and ultimately transitions to a de Sitter phase.

The critical points, eigenvalues, stability of the critical points, and deceleration parameter are summarized in Table 3. The phase space diagram for this scenario is illustrated in Fig. 11. The figure indicates that critical point A acts as a saddle point since certain trajectories converge towards it while others stray away. At this significant stage, the effect of matter is greater than that of dark energy, indicating a phase of deceleration. Critical point B functions as a future attractor, as trajectories converge towards it. In this critical stage, dark energy takes precedence over matter, leading to a phase of acceleration. Therefore, the analysis of the phase plot in this instance implies a universe that originates from

Table 3 Critical points of the autonomous system described by Eqs. (48a) and (48b) for the model

Parameter Set	Critical Point	Eigenvalue	Stability	q
CC	A $\rightarrow$ (1.069, -0.069)	$\{-0.081, 3.131\}$	Saddle	0.467
	B $\rightarrow$ (-0.040, 1.040)	$\{-0.081, -3.131\}$	Stable	-1.098
Pantheon	A $\rightarrow$ (1.070, -0.070)	$\{-0.087, 3.038\}$	Saddle	0.423
	B $\rightarrow$ (-0.038, 1.038)	$\{-0.087, -3.038\}$	Stable	-1.097
Pantheon+CC	A $\rightarrow$ (1.068, -0.068)	$\{-0.09, 3.126\}$	Saddle	0.466
	B $\rightarrow$ (-0.036, 1.036)	$\{-0.09, -3.126\}$	Stable	-1.096

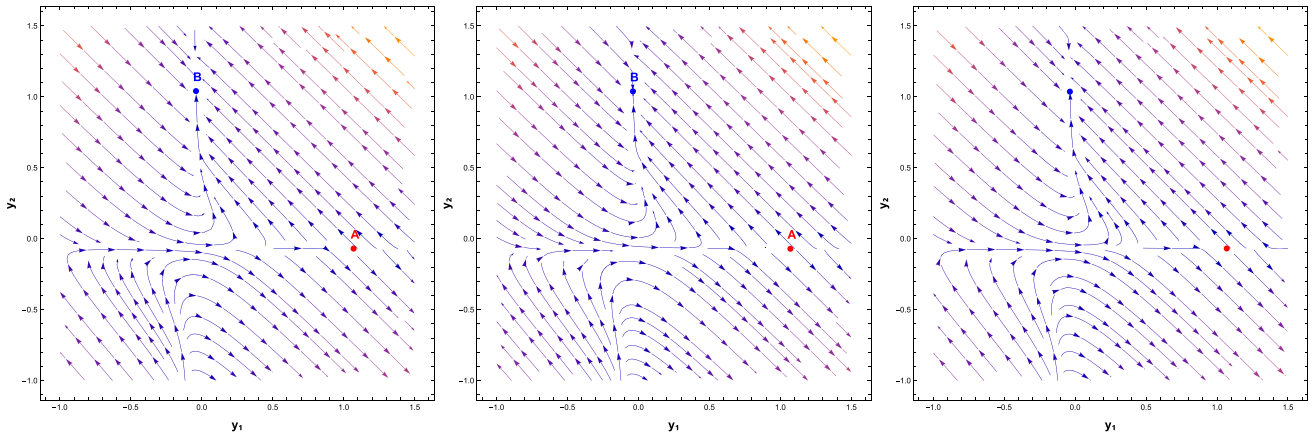

Fig. 11 The phase space configuration in the $y_1 - y_2$ plane is presented for the *CC* data (left panel), the *Pantheon* data set (middle panel), and the *Pantheon*+CC data set (right panel). The saddle is represented by a red circle, and a blue solid circle denotes the future attractor. The trajectories' direction is shown by the arrowhead

matter-dominated conditions and culminates in a de-Sitter-type universe.

7 Conclusion

In this article, we have investigated a viable cosmological model characterized by bulk viscosity and a decaying vacuum density, which are interpreted as dark matter and dark energy within a spatially FLRW spacetime. The presence of DM and DE necessitates an interaction between these components. The coupling between the viscous fluid and the vacuum energy density is established through a coupling parameter, denoted as Q. In the absence of a definitive fundamental physical theory, the most frequently examined interacting terms in the literature are $Q \propto \rho_m H$ or $Q \propto \rho_\Lambda H$. We have opted to define the coupling term as a combination of both, specifically $Q = 3H\alpha(\rho_m + \rho_\Lambda)$. In our analysis, we have considered that the non-equilibrium bulk viscous pressure adheres to the elementary Eckart's theory, expressed as $\Pi = -3\zeta H$. Due to the absence of a well-established theory for the functional form of the bulk viscous coefficient, it is significant to note that the viscosity is dependent upon the Universe's expansion rate. Consequently, we have employed a more contemporary expression as referenced in [41,42], which is formulated as $\zeta = \zeta_1 H + \zeta_0 \rho_m H^{-1}$. Similarly, the motivation for the VED derived from the general covariance of the effective action in quantum field theory, represented as $\rho_\Lambda = C_0 + 3\nu H^2$. In the subsequent section, we summarize the main points of our analysis.

In the first segment of our research, we derived the model equation and obtained its analytical solution in terms of redshift. Subsequently, we executed a MCMC analysis to constrain the model parameters through the chi-squared minimization method. Our study utilizes two observational datasets: the *CC* dataset and the Type Ia Supernova *Pantheon* dataset, comprising 31 and 1, 048 data points, respectively. We also incorporated the *Pantheon* + CC dataset. We adopted the ΛCDM model as our reference, which enables us to assess the consistency or discrepancies between the model's predictions and observational data, thereby providing insights into the model's viability. The constrained values for the optimal model parameters are shown in Table 1. From the table 1, it is evident that the tension in the H_0 measurement is almost alleviated in the proposed model in comparison to Planck 2018 and $R21$. Observations reveal that the reduced chi-squared value, χ^2_{red}, is under one for each data set, suggesting that the model fits the observational data exceptionally well. Addi-

tionally, the evaluation of information criteria, especially the ΔAIC value indicates strong support but ΔBIC values, suggest that this model is less preferred compared to the ΛCDM model.

From the perspective of observational consistency, we have analyzed the evolutionary characteristics of several cosmological parameters, including the deceleration parameter, effective equation of state, the statefinder pairs, and the Om diagnostic, and have determined their current values given in Table 2. In particular, for the deceleration parameter, we obtained $q_0 = -0.494^{+0.173}_{-0.244}$, $q_0 = -0.500^{+0.174}_{-0.234}$, and $-0.504^{+0.175}_{-0.235}$ from the $H(z)$ data, *Pantheon* sample, and *Pantheon*+CC, respectively. As z approaches -1, the model aligns with the ΛCDM model, where $\omega = -1$, signifies a shift to the de Sitter phase in the late universe displayed in Fig. 5. The proposed model exhibits a small negative value for the equation of state parameter at high redshifts and asymptotically approaches a cosmological constant at low redshifts. Consequently, the model behaves like a quintessence in the early universe and resembles a cosmological constant in later times. Figure 6 illustrates that the r-s evolution is projected to converge with the ΛCDM point in the future, while the current values of the statefinder pairs indicate that our model diverges from existing dark energy models. According to the Om diagnostic test (Fig. 7), our model exhibits characteristics akin to quintessence. The estimated age of the universe for this model is well inside the range 12.9 ± 2.9 Gyr and 13.79 Gyr obtained from the oldest globular clusters and Planck [149,172].

Our findings reveal that critical point A functions as a saddle point, with the deceleration parameter nearing $1/2$. In contrast, critical point B operates as a future attractor, where the deceleration parameter is $q = -1$. This suggests a phase dominated by matter, ultimately transitioning into a late-time phase governed by dark energy. We have not included radiation in our current analysis but we plan to address this in future studies.

The stability of the universe, when viewed through a thermodynamic lens, along with the affirmation of the Generalized Second Law, is supported by an analysis of entropy dynamics within the framework of an expanding universe. Figure 10 illustrates that $S'' > 0$ during the initial evolutionary stage, which subsequently shifts to $S'' < 0$ in the more recent past, nearing the transition redshift. As a result, we can deduce that the universe continually adheres to the Generalized Second Law throughout its evolutionary journey.

While our work builds on previous studies such as Ref. [42,106], it introduces several key innovations that go beyond incremental changes. Most notably, we adopt a more general bulk viscosity form and a distinct interaction term, leading to qualitatively different cosmological dynamics. Specifically, we consider the recently introduced viscosity coefficient $\zeta = \zeta_0 H + \zeta_1 \rho_m H^{-1}$, as in Ref. [42], along with the interaction term $Q = 3H\alpha(\rho_m + \rho_\Lambda)$, different form that studided in Ref. [42,106]. In Ref. [42], the author studied the late acceleration of the universe in the context of $f(R,T)$ gravity in near equlibrium condition with bulk viscous matter (bulk viscosity, $\zeta = \zeta_0 H + \zeta_1 \rho_m H^{-1}$). They have not considered cosmological constant or dark energy and any form of interaction. In our study we focus a cosmological model in which the Universe is conceptualized as comprising two primary components, dark energy and matter and also their interaction. We demonstrate that the combination of this viscous formulation, variable VED, and interaction term is capable of producing late-time cosmic acceleration-an outcome explicitly obtained in our analysis. A significant novel contribution of our paper is the inclusion of a detailed thermodynamic investigation, particularly examining the evolution of entropy and validating the GSL within this interacting viscous framework-an aspect not explored in earlier studies. In addition, we present a comprehensive phase space analysis, which was not included in Ref. [106], offering new insights into the stability and asymptotic behavior of the cosmological solutions. We also note that while Ref. [188] studies a bulk viscous matter universe with a cosmological constant Λ, it does not report results for several cosmological parameters. In contrast, our model predicts quantities such as the deceleration parameter and the age of the universe. Although these results remain close to those of ΛCDM due to the smallness of the viscosity coefficient fitted from SNe Ia data, our model nonetheless provides a consistent and extended framework. Importantly, we find that the predicted Hubble parameter values in our model nearly resolve the current Hubble tension, yielding compatible results with both the local measurement by R21 and the global estimate by the *Planck* collaboration. Taken together, these theoretical and phenomenological advancements clearly distinguish our work from prior literature. As a final point, it is essential to note that interacting viscous models incorporating decaying VED could be favored as viable candidates for examining dark energy models that surpass the standard cosmological constant. This model is adequately equipped to elucidate the dynamical aspects of the universe and its present acceleration.

Funding The authors wish to clarify that they have not received funding from institutional projects while preparing this article.

Data Availability Statement Data sharing does not apply to this article since no datasets were produced or examined in the course of this study.

Code Availability Statement Code/Software sharing is not applicable to this article, as the current study did not involve generating or analyzing any code or software.

Declarations

Conflict of interest The authors state that there are no conflict of interest.

Funded by SCOAP[3].

References

1. S. Alam, M. Ata, S. Bailey, F. Beutler, D. Bizyaev, J.A. Blazek, A.S. Bolton, J.R. Brownstein, A. Burden, C.-H. Chuang et al., Mon. Not. R. Astron. Soc. **470**, 2617 (2017)
2. M.H. Amante, J. Magana, V. Motta, M.A. García-Aspeitia, T. Verdugo, Mon. Not. R. Astron. Soc. **498**, 6013 (2020)
3. S. Perlmutter, G. Aldering, G. Goldhaber, R.A. Knop, P. Nugent, P.G. Castro, S. Deustua, S. Fabbro, A. Goobar, D.E. Groom, I.M. Hook, A.G. Kim, M.Y. Kim, J.C. Lee, N.J. Nunes, R. Pain, C.R. Pennypacker, R. Quimby, C. Lidman, R.S. Ellis, M. Irwin, R.G. McMahon, P. Ruiz-Lapuente, N. Walton, B. Schaefer, B.J. Boyle, A.V. Filippenko, T. Matheson, A.S. Fruchter, N. Panagia, H.J.M. Newberg, W.J. Couch, T. S. C. Project, Astrophys. J. **517**, 565–586 (1999). https://doi.org/10.1086/307221
4. A.G. Riess, A.V. Filippenko, P. Challis, A. Clocchiatti, A. Diercks, P.M. Garnavich, R.L. Gilliland, C.J. Hogan, S. Jha, R.P. Kirshner et al., Astron. J. **116**, 1009 (1998)
5. A.G. Riess, L.-G. Strolger, J. Tonry, S. Casertano, H.C. Ferguson, B. Mobasher, P. Challis, A.V. Filippenko, S. Jha, W. Li et al., Astrophys. J. **607**, 665 (2004)
6. V. Springel, C.S. Frenk, S.D. White, Nature **440**, 1137 (2006)
7. S.W. Hawking, G.F. Ellis, *The Large Scale Structure of Space-time* (Cambridge University Press, Cambridge, 2023)
8. E. Komatsu, J. Dunkley, M. Nolta, C.L. Bennett, B. Gold, G. Hinshaw, N. Jarosik, D. Larson, M. Limon, L. Page et al., Astrophys. J. Suppl. Ser. **180**, 330 (2009)
9. D.J. Eisenstein, I. Zehavi, D.W. Hogg, R. Scoccimarro, M.R. Blanton, R.C. Nichol, R. Scranton, H.-J. Seo, M. Tegmark, Z. Zheng et al., Astrophys. J. **633**, 560 (2005)
10. N.J. Mohan, A. Sasidharan, T.K. Mathew, Eur. Phys. J. C **77**, 1 (2017)
11. S. Hanany, P. Ade, A. Balbi, J. Bock, J. Borrill, A. Boscaleri, P. de Bernardis, P. Ferreira, V. Hristov, A.H. Jaffe et al., Astrophys. J. **545**, L5 (2000)
12. D.N. Spergel, R. Bean, O. Doré, M. Nolta, C. Bennett, J. Dunkley, G. Hinshaw, N.E. Jarosik, E. Komatsu, L. Page et al., Astrophys. J. Suppl. Ser. **170**, 377 (2007)
13. M. Tegmark, M.A. Strauss, M.R. Blanton, K. Abazajian, S. Dodelson, H. Sandvik, X. Wang, D.H. Weinberg, I. Zehavi, N.A. Bahcall et al., Phys. Rev. D **69**, 103501 (2004)
14. M. Tegmark, M.R. Blanton, M.A. Strauss, F. Hoyle, D. Schlegel, R. Scoccimarro, M.S. Vogeley, D.H. Weinberg, I. Zehavi, A. Berlind et al., Astrophys. J. **606**, 702 (2004)
15. M. Setare, E.C. Vagenas, Phys. Lett. B **666**, 111 (2008)
16. S.M. Carroll, Living Rev. Relativ. **4**, 1 (2001)
17. S. Weinberg, Rev. Mod. Phys. **61**, 1 (1989)
18. T. Padmanabhan, Phys. Rep. **380**, 235 (2003)
19. H.E. Velten, R.F. vom Marttens, W. Zimdahl, Eur. Phys. J. C **74**, 1 (2014)
20. M. Pietroni, Phys. Rev. D **67**, 103523 (2003)
21. J.R. Wilson, G.J. Mathews, G.M. Fuller, Phys. Rev. D-Part. Fields Gravit. Cosmol. **75**, 043521 (2007)
22. H. Okumura, F. Yonezawa, Physica A Stat. Mech. Appl. **321**, 207 (2003)
23. T. Harko, M. Mak, Int. J. Mod. Phys. D **9**, 97 (2000)
24. W. Zimdahl, Mon. Not. R. Astron. Soc. **280**, 1239 (1996)
25. A. Avelino, U. Nucamendi, J. Cosmol. Astropart. Phys. **2009**(04), 006
26. P. Ilg, H.C. Öttinger, Phys. Rev. D **61**, 023510 (1999)
27. D. Pavon, W. Zimdahl, Phys. Lett. A **179**, 261 (1993)
28. J. Wang, X. Meng, Mod. Phys. Lett. A **29**, 1450009 (2014)
29. C. Eckart, Phys. Rev. **58**, 919 (1940)
30. L.D. Landau, E.M. Lifshitz, *Fluid Mechanics*, vol. 6 (Elsevier, Amsterdam, 1987)
31. W. Israel, J. Stewart, Phys. Lett. A **58**, 213 (1976)
32. S. Weinberg, *Gravitation and Cosmology: Principles and Applications of the General Theory of Relativity* (Wiley, New York, 2013)
33. G.L. Murphy, Phys. Rev. D **8**, 4231 (1973)
34. N. Cruz, E. González, J. Jovel, Phys. Rev. D **105**, 024047 (2022)
35. S. Lepe, G. Otalora, J. Saavedra, Phys. Rev. D **96**, 023536 (2017)
36. N.J. Mohan, P. Krishna, A. Sasidharan, T.K. Mathew, Class. Quantum Gravity **37**, 075007 (2020)
37. G. Acquaviva, A. Beesham, Class. Quantum Gravity **32**, 215026 (2015)
38. G. Gómez, G. Palma, E. González, Á. Rincón, N. Cruz, Eur. Phys. J. Plus **138**, 738 (2023)
39. J. Ren, X.-H. Meng, Phys. Lett. B **633**, 1 (2006)
40. M. Xin-He, D. Xu, Commun. Theor. Phys. **52**, 377 (2009)
41. D.S. Rana, P. Sahoo, Gen. Relativ. Gravit. **56**, 82 (2024)
42. V.A. Pai, T.K. Mathew, Class. Quantum Gravity **41**, 085002 (2024)
43. O. Bertolami, Nuovo Cimento B Serie **93B**, 36 (1986). https://doi.org/10.1007/BF02728301
44. M. Özer, M. Taha, Nucl. Phys. B **287**, 776 (1987)
45. M. Rezaei, M. Malekjani, J.S. Peracaula, Phys. Rev. D **100**, 023539 (2019)
46. C.P. Singh, J. Solà Peracaula, Eur. Phys. J. C (2021). https://doi.org/10.1140/epjc/s10052-021-09765-7
47. V. Khatri, C. Singh, Astrophys. Space Sci. **368**, 16 (2023)
48. P. Wang, X.-H. Meng, Class. Quantum Gravity **22**, 283 (2004)
49. F. Costa, J. Alcaniz, Phys. Rev. D-Part. Fields Gravit. Cosmol. **81**, 043506 (2010)
50. J. Sola, H. Štefančić, Mod. Phys. Lett. A **21**, 479 (2006)
51. J. Sola, A. Gomez-Valent, Int. J. Mod. Phys. D **24**, 1541003 (2015)
52. A. Jayadevan, M. Mukesh, A. Shaima, T.K. Mathew, Astrophys. Space Sci. **364**, 1 (2019)
53. I.L. Shapiro, J. Sola, J. High Energy Phys. **2002**, 006 (2002)
54. J. Sola, J. Phys. A: Math. Theor. **41**, 164066 (2008)
55. A. Bonanno, M. Reuter, Phys. Rev. D (2002). https://doi.org/10.1103/physrevd.65.043508
56. M. Reuter, Phys. Rev. D **57**, 971–985 (1998). https://doi.org/10.1103/physrevd.57.971
57. S. Basilakos, J.A.S. Lima, J. Sola, Int. J. Mod. Phys. D **22**, 1342008 (2013)
58. A. Babić, B. Guberina, R. Horvat, H. Štefančić, Phys. Rev. D **65**, 085002 (2002)
59. J.A. P, M. M, S. Akbar, T.K. Mathew, Astrophys. Space Sci. **364**, 67 (2019). https://doi.org/10.1007/s10509-019-3550-z. arXiv:1808.07729 [gr-qc]
60. J. Solà, A. Gómez-Valent, J. de Cruz Pérez, Int. J. Mod. Phys. A **32**, 1730014 (2017)

61. J. Solà Peracaula, Int. J. Mod. Phys. D **27**, 1847029 (2018). https://doi.org/10.1142/S0218271818470296. arXiv:1805.09810 [gr-qc]
62. S. Basilakos, M. Plionis, J. Solà, Phys. Rev. D **80**, 083511 (2009). https://doi.org/10.1103/PhysRevD.80.083511. arXiv:0907.4555 [astro-ph.CO]
63. D. Bessada, O.D. Miranda, Phys. Rev. D **88**, 083530 (2013). https://doi.org/10.1103/PhysRevD.88.083530. arXiv:1310.8571 [gr-qc]
64. C. Singh, Nuovo Cimento B Serie **122**, 89 (2007)
65. C. Singh, S. Kumar, Astrophys. Space Sci. **323**, 407 (2009)
66. N. Mostafapoor, Ø. Grøn, Astrophys. Space Sci. **333**, 357 (2011)
67. J. Hu, H. Hu, Eur. Phys. J. Plus (2020). https://doi.org/10.1140/epjp/s13360-020-00623-1
68. L. Herrera-Zamorano, A. Hernández-Almada, M.A. García-Aspeitia, Eur. Phys. J. C **80**, 637 (2020)
69. R. Murgia, S. Gariazzo, N. Fornengo, J. Cosmol. Astropart. Phys. **04**, 014 (2016)
70. J. Väliviita, E. Palmgren, J. Cosmol. Astropart. Phys. **07**, 015 (2015)
71. M.A. Buen-Abad, R. Essig, D. McKeen, Y.-M. Zhong, Phys. Rep. **961**, 1–35 (2022). https://doi.org/10.1016/j.physrep.2022.02.006
72. K. Hagiwara, K. Hikasa, K. Nakamura, M. Tanabashi, M. Aguilar-Benitez, C. Amsler, R. Barnett, P. Burchat, C. Carone, C. Caso et al., Phys. Rev. D (Part. Fields) **66** (2002)
73. N. Tamanini, Phys. Rev. D **92**, 043524 (2015)
74. B. Wang, E. Abdalla, F. Atrio-Barandela, D. Pavón, Rep. Prog. Phys. **79**, 096901 (2016). https://doi.org/10.1088/0034-4885/79/9/096901
75. P. Brax, J. Martin, Phys. Lett. B **468**, 40–45 (1999). https://doi.org/10.1016/s0370-2693(99)01209-5
76. E. Elizalde, S. Nojiri, S.D. Odintsov, Phys. Rev. D (2004). https://doi.org/10.1103/physrevd.70.043539
77. Y. Li, J. Ma, J. Cui, Z. Wang, X. Zhang, Sci. China Phys. Mech. Astron. **54**, 1367 (2011)
78. J.A. Frieman, B.-A. Gradwohl, Phys. Rev. Lett. **67**, 2926 (1991)
79. S.-S. Xue, Nucl. Phys. B **897**, 326 (2015)
80. L. Amendola, Phys. Rev. D (1999). https://doi.org/10.1103/physrevd.60.043501
81. B.-A. Gradwohl, J.A. Frieman, Astrophys. J. Part 1 **398**(2), 407–424 (1992)
82. S.H. Pereira, J.F. Jesus, Phys. Rev. D (2009). https://doi.org/10.1103/physrevd.79.043517
83. C.-Y. Sun, R.-H. Yue, Phys. Rev. D (2012). https://doi.org/10.1103/physrevd.85.043010
84. Y.-H. Li, X. Zhang, Eur. Phys. J. C (2011). https://doi.org/10.1140/epjc/s10052-011-1700-8
85. K. Koyama, R. Maartens, Y.-S. Song, J. Cosmol. Astropart. Phys. **2009**(10), 017
86. C.G. Boehmer, G. Caldera-Cabral, R. Lazkoz, R. Maartens, Phys. Rev. D-Part. Fields Gravit. Cosmol. **78**, 023505 (2008)
87. A.P. Billyard, A.A. Coley, Phys. Rev. D **61**, 083503 (2000)
88. M. Sharif, S. Jabbar, Commun. Theor. Phys. **63**, 168 (2015)
89. G. Olivares, F. Atrio-Barandela, D. Pavon, Phys. Rev. D-Part. Fields Gravit. Cosmol. **71**, 063523 (2005)
90. E. Abdalla, L.R. Abramo, L. Sodré Jr., B. Wang, Phys. Lett. B **673**, 107 (2009)
91. L. Amendola, G.C. Campos, R. Rosenfeld, Phys. Rev. D-Part. Fields Gravit. Cosmol. **75**, 083506 (2007)
92. Z.-K. Guo, N. Ohta, S. Tsujikawa, Phys. Rev. D-Part. Fields Gravit. Cosmol. **76**, 023508 (2007)
93. D. Pavón, B. Wang, Gen. Relativ. Gravit. **41**, 1 (2009)
94. M. Quartin, M.O. Calvao, S.E. Joras, R.R. Reis, I. Waga, J. Cosmol. Astropart. Phys. **2008**(05), 007
95. B. Wang, Y. Gong, E. Abdalla, Phys. Lett. B **624**, 141 (2005)
96. J. Väliviita, J. Cosmol. Astropart. Phys. **2017**(04), 014
97. S. Nojiri, S.D. Odintsov, Phys. Rep. **505**, 59 (2011)
98. I. Brevik, V. Obukhov, A. Timoshkin, Astrophys. Space Sci. **355**, 399 (2015)
99. G. Caldera-Cabral, R. Maartens, L.A. Urena-Lopez, Phys. Rev. D-Part. Fields Gravit. Cosmol. **79**, 063518 (2009)
100. J.-J. Geng, Y.-H. Li, J.-F. Zhang, X. Zhang, Eur. Phys. J. C **75**, 356 (2015)
101. D.G. Duniya, D. Bertacca, R. Maartens, Phys. Rev. D **91**, 063530 (2015)
102. K.A. Malik, D. Wands, C. Ungarelli, Phys. Rev. D **67**, 063516 (2003)
103. F. Ferrer, S. Räsänen, J. Väliviita, J. Cosmol. Astropart. Phys. **2004**(10), 010
104. H. Assadullahi, J. Väliviita, D. Wands, Phys. Rev. D-Part. Fields Gravit. Cosmol. **76**, 103003 (2007)
105. F. Simpson, Phys. Rev. D-Part. Fields Gravit. Cosmol. **82**, 083505 (2010)
106. V. Khatri, C.P. Singh, M. Srivastava, Exploring interacting bulk viscous model with decaying vacuum density. (2024). arXiv:2405.15296 [astro-ph.CO]
107. D. Foreman-Mackey, D.W. Hogg, D. Lang, J. Goodman, Publ. Astron. Soc. Pac. **125**, 306 (2013)
108. D.M. Scolnic, D. Jones, A. Rest, Y. Pan, R. Chornock, R. Foley, M. Huber, R. Kessler, G. Narayan, A. Riess et al., Astrophys. J. **859**, 101 (2018)
109. M. Sharif, S. Mumtaz, Astrophys. Space Sci. **362**, 205 (2017)
110. A.A. Coley, *Dynamical Systems and Cosmology*, vol. 291 (Springer Science & Business Media, Berlin, 2013)
111. J. Wainwright, G.F.R. Ellis, *Dynamical Systems in Cosmology* (1997)
112. C.G. Böhmer, N. Chan, *Dynamical and Complex Systems* (World Scientific, Singapore, 2017), pp.121–156
113. R. García-Salcedo, T. Gonzalez, F.A. Horta-Rangel, I. Quiros, D. Sanchez-Guzmán, Eur. J. Phys. **36**, 025008 (2015)
114. F. Melia, Mod. Phys. Lett. A **37**, 2250016 (2022)
115. S. Nojiri, S.D. Odintsov, S. Tsujikawa, Phys. Rev. D-Part. Fields Gravit. Cosmol. **71**, 063004 (2005)
116. G. Barnaföldi, V. Gogokhia, J. Phys. G: Nucl. Part. Phys. **37**, 025003 (2010)
117. E.B. Manoukian, Phys. Rev. D **27**, 1299 (1983)
118. A. Beesham, R.K. Tiwari, in *Journal of Physics: Conference Series*, vol. 1557 (IOP Publishing, 2020), p. 012001
119. J. Garriga, A. Vilenkin, Phys. Rev. D **64**, 023517 (2001)
120. L. Lombriser, Phys. Lett. B **797**, 134804 (2019)
121. A. Gelman, J.B. Carlin, H.S. Stern, D.B. Rubin, *Bayesian Data Analysis* (Chapman and Hall/CRC, Boca Raton, 1995)
122. D. Arora, H. Chaudhary, S.K.J. Pacif, G. Mustafa, Eur. Phys. J. Plus **139**, 371 (2024)
123. A. Lewis, S. Bridle, Phys. Rev. D **66**, 103511 (2002)
124. M. Tegmark, A.N. Taylor, A.F. Heavens, Astrophys. J. **480**, 22 (1997)
125. M. Kowalski, D. Rubin, G. Aldering, R. Agostinho, A. Amadon, R. Amanullah, C. Balland, K. Barbary, G. Blanc, P.J. Challis et al., Astrophys. J. **686**, 749 (2008)
126. R. Amanullah, C. Lidman, D. Rubin, G. Aldering, P. Astier, K. Barbary, M. Burns, A. Conley, K. Dawson, S. Deustua et al., Astrophys. J. **716**, 712 (2010)
127. N. Suzuki, D. Rubin, C. Lidman, G. Aldering, R. Amanullah, K. Barbary, L. Barrientos, J. Botyanszki, M. Brodwin, N. Connolly et al., Astrophys. J. **746**, 85 (2012)
128. Z. Chang, D. Zhao, Y. Zhou, Chin. Phys. C **43**, 125102 (2019)
129. H.E. Flewelling, E. Magnier, K. Chambers, J. Heasley, C. Holmberg, M. Huber, W. Sweeney, C. Waters, A. Calamida, S. Casertano et al., Astrophys. J. Suppl. Ser. **251**, 7 (2020)

130. J.A. Frieman, B. Bassett, A. Becker, C. Choi, D. Cinabro, F. DeJongh, D.L. Depoy, B. Dilday, M. Doi, P.M. Garnavich et al., Astron. J. **135**, 338 (2007)
131. P. Astier, J. Guy, N. Regnault, R. Pain, E. Aubourg, D. Balam, S. Basa, R. Carlberg, S. Fabbro, D. Fouchez et al., Astron. Astrophys. **447**, 31 (2006)
132. P.M. Garnavich, R.P. Kirshner, P. Challis, J. Tonry, R.L. Gilliland, R.C. Smith, A. Clocchiatti, A. Diercks, A.V. Filippenko, M. Hamuy et al., Astrophys. J. **493**, L53 (1998)
133. G.F. Ellis, R. Maartens, M.A. MacCallum, *Relativistic Cosmology* (Cambridge University Press, Cambridge, 2012)
134. R. Arjona, W. Cardona, S. Nesseris, Phys. Rev. D **99**, 043516 (2019)
135. D.C. Maurya, R. Myrzakulov, Eur. Phys. J. C **84**, 625 (2024)
136. M. Moresco, L. Amati, L. Amendola, S. Birrer, J.P. Blakeslee, M. Cantiello, A. Cimatti, J. Darling, M. Della Valle, M. Fishbach et al., Living Rev. Relativ. **25**, 6 (2022)
137. E. Gaztanaga, C. Bonvin, L. Hui, J. Cosmol. Astropart. Phys. **2017**(01), 032
138. J.-C. Zhang, J. Zheng, T.-J. Zhang, Astrophys. J. **928**, 4 (2022). https://doi.org/10.3847/1538-4357/ac549c
139. K.P. Bumham, D.R. Anderson, (Springer, New York, 2002)
140. H. Akaike, IEEE Trans. Autom. Control **19**, 716 (1974)
141. G. Schwarz, Ann. Stat. 461 (1978)
142. K.P. Burnham, D.R. Anderson, Sociol. Methods Res. **33**, 261 (2004)
143. A.R. Liddle, Mon. Not. Roy. Astron. Soc. Lett. **377**, L74 (2007)
144. H. Jeffreys, *The Theory of Probability* (OuP, Oxford, 1998)
145. F.K. Anagnostopoulos, S. Basilakos, E.N. Saridakis, Phys. Rev. D **103**, 104013 (2021)
146. J. Akeret, S. Seehars, A. Amara, A. Refregier, A. Csillaghy, Astron. Comput. **2**, 27–39 (2013). https://doi.org/10.1016/j.ascom.2013.06.003
147. R. Briffa, C. Escamilla-Rivera, J.L. Said, J. Mifsud, Mon. Not. R. Astron. Soc. **522**, 6024–6034 (2023). https://doi.org/10.1093/mnras/stad1384
148. Bennett et al., Astrophys J Suppl Ser **208**, 20 (2013)
149. Y.N. Aghanim, F. Arroja, J. Aumont, C. Baccigalupi, M. Ballardini, A. Banday, N.R.B. Barreiro, S. Basak, R. Battye, K. Benabed et al., Astron. Astrophys. **641** (2020)
150. P. Ade, N. Aghanim, M. Arnaud, M. Ashdown, J. Aumont, C. Baccigalupi, A.J. Banday, R. Barreiro, J. Bartlett, E. Battaner et al., Astron. Astrophys. **566**, A54 (2014)
151. P. Collaboration, N. Aghanim, Y. Akrami, F. Arroja, M. Ashdown, J. Aumont, C. Baccigalupi, M. Ballardini, A. Banday, R. Barreiro et al., A&A **641**, A1 (2020)
152. W.L. Freedman, B.F. Madore, B.K. Gibson, L. Ferrarese, D.D. Kelson, S. Sakai, J.R. Mould, R.C. Kennicutt Jr., H.C. Ford, J.A. Graham et al., Astrophys. J. **553**, 47 (2001)
153. W.L. Freedman, B.F. Madore, V. Scowcroft, C. Burns, A. Monson, S.E. Persson, M. Seibert, J. Rigby, Astrophys. J. **758**, 24 (2012)
154. A.G. Riess, W. Yuan, L.M. Macri, D. Scolnic, D. Brout, S. Casertano, D.O. Jones, Y. Murakami, G.S. Anand, L. Breuval et al., Astrophys. J. Lett. **934**, L7 (2022)
155. J.-P. Hu, F.-Y. Wang, Universe **9**, 94 (2023)
156. Y.L. Bolotin, V. Cherkaskiy, O. Lemets, D. Yerokhin, L. Zazunov, arXiv preprint arXiv:1502.00811 (2015)
157. U. Alam, V. Sahni, A.A. Starobinsky, J. Cosmol. Astropart. Phys. **2004**(06), 008
158. S. Del Campo, I. Duran, R. Herrera, D. Pavon, Phys. Rev. D-Part. Fields Gravit. Cosmol. **86**, 083509 (2012)
159. D. Wang, M. Koussour, A. Malik, N. Myrzakulov, G. Mustafa, Eur. Phys. J. C **83**, 670 (2023)
160. M. Koussour, Chin. J. Phys. **83**, 454 (2023)
161. U. Alam, V. Sahni, A.A. Starobinsky, J. Cosmol. Astropart. Phys. **2004**(06), 008. https://doi.org/10.1088/1475-7516/2004/06/008
162. R. Colistete, J.C. Fabris, J. Tossa, W. Zimdahl, Phys. Rev. D (2007). https://doi.org/10.1103/physrevd.76.103516
163. N. Ahmed, S.Z. Alamri, Int. J. Geom. Methods Mod. Phys. **16**, 1950159 (2019)
164. D.M. Gusu, Adv. High Energy Phys. **2020**, 4015426 (2020)
165. V. Sahni, T.D. Saini, A.A. Starobinsky, U. Alam, J. Exp. Theor. Phys. Lett. **77**, 201 (2003)
166. C.-J. Feng, Phys. Lett. B **670**, 231 (2008)
167. P. Wu, H. Yu, Phys. Lett. B **693**, 415 (2010)
168. R. Carrasco, A. Rincon, J. Saavedra, N. Videla, Discriminating interacting dark energy models using statefinder diagnostic. (2023). arXiv:2310.04324 [gr-qc]
169. V. Sahni, A. Shafieloo, A.A. Starobinsky, Phys. Rev. D-Part. Fields Gravit. Cosmol. **78**, 103502 (2008)
170. M.-L. Tong, Y. Zhang, Phys. Rev. D-Part. Fields Gravit. Cosmol. **80**, 023503 (2009)
171. U. Debnath, S. Chattopadhyay, Int. J. Theor. Phys. **52**, 1250 (2013)
172. A.G. Riess, S. Casertano, W. Yuan, L.M. Macri, D. Scolnic, Astrophys. J. **876**, 85 (2019)
173. R. Criss, A. Hofmeister, Geochim. Cosmochim. Acta **65**, 4077 (2001)
174. M.T. Manoharan, N. Shaji, T.K. Mathew, Eur. Phys. J. C **83**, 19 (2023)
175. C.A. Egan, C.H. Lineweaver, Astrophys. J. **710**, 1825 (2010)
176. T.K. Mathew et al., arXiv preprint arXiv:2204.12097 (2022)
177. K. Karami, S. Ghaffari, Phys. Lett. B **688**, 125 (2010)
178. P. Krishna, T.K. Mathew, Phys. Rev. D **96**, 063513 (2017)
179. S. Kadam, N.P. Thakkar, B. Mishra, Eur. Phys. J. C **83**, 809 (2023)
180. E.J. Copeland, A.R. Liddle, D. Wands, Phys. Rev. D **57**, 4686 (1998)
181. C.R. Fadragas, G. Leon, Class. Quantum Gravity **31**, 195011 (2014)
182. S. Wiggins, *Introduction to Applied Nonlinear Dynamical Systems and Chaos [electronic resource]* (Astronomy and Astrophysics Library, Springer, New York, 1990). https://doi.org/10.1007/978-1-4757-4067-7
183. M.A. Savi, in *Dynamics of Smart Systems and Structures: Concepts and Applications*, vol. 93 (2016)
184. G. Papagiannopoulos, P. Tsiapi, S. Basilakos, A. Paliathanasis, Eur. Phys. J. C **80**, 55 (2020)
185. A. Avelino, R. García-Salcedo, T. Gonzalez, U. Nucamendi, I. Quiros, J. Cosmol. Astropart. Phys. **2013**, 012 (08)
186. S. Basilakos, G. Leon, G. Papagiannopoulos, E.N. Saridakis, Phys. Rev. D (2019). https://doi.org/10.1103/physrevd.100.043524
187. E.J. Copeland, M. Sami, S. Tsujikawa, Int. J. Mod. Phys. D **15**, 1753–1935 (2006). https://doi.org/10.1142/s021827180600942x
188. J. Hu, H. Hu, Eur. Phys. J. Plus **135**, 1 (2020)